

NAG5-842

IN-46-CR

154838

608.

**Effects of a Temperature-Dependent Rheology
on Large Scale Continental Extension**

(NASA-CR-183117) EFFECTS OF A
TEMPERATURE-DEPENDENT RHEOLOGY ON LARGE
SCALE CONTINENTAL EXTENSION (California
Inst. of Tech.) 60 p CSCL 08E

N88-26759

Unclas

G3/46 · 0154838

Leslie J. Sonder

Seismological Laboratory, 252-21
California Institute of Technology,
Pasadena, CA. 91125

and

Philip C. England

Department of Earth Sciences,
Parks Road,
University of Oxford,
Oxford OX1 3PR
England

Abstract

The effects of a temperature-dependent rheology on large-scale continental extension are investigated using a thin viscous sheet model. A vertically-averaged rheology is used that is consistent with laboratory experiments on power-law creep of olivine and that depends exponentially on temperature. Results of the calculations depend principally on two parameters: the Peclet number, which describes the relative rates of advection and diffusion of heat, and a dimensionless activation energy, which controls the temperature dependence of the rheology. At short times following the beginning of extension, deformation occurs with negligible change in temperature, so that only small changes in lithospheric strength occur due to attenuation of the lithosphere. However, after a certain critical time interval, thermal diffusion lowers temperatures in the lithosphere, strongly increasing lithospheric strength and slowing the rate of extension. This critical time depends principally on the Peclet number and is short compared with the thermal time constant of the lithosphere. The strength changes cause the locus of high extensional strain rates to shift with time from regions of high strain to regions of low strain. Results of the calculations are compared with observations from the Aegean, where maximum extensional strains are found in the south, near Crete, but maximum present-day strain rates are largest about 300 km further north. The comparisons support the hypothesis that the observed separation of the loci of maximum strain and maximum present-day strain rates in the Aegean may be the consequence of changes in lithospheric strength arising from the temperature-dependent mechanical properties of lithospheric materials.

1. Introduction

Recently, much attention has been directed towards understanding continental extensional tectonics. Simple kinematic models of stretching continental lithosphere (e.g., McKenzie, 1978a; Jarvis and McKenzie, 1980; Royden and Keen, 1980) have been shown to be consistent with the subsidence histories of a number of sedimentary basins and passive margins (e.g. Sclater and Christie, 1980; Royden and Keen, 1980; Le Pichon and Sibuet, 1981; Royden et al., 1983). In these models, horizontal stretching of the lithosphere (and attendant vertical thinning) perturbs the geotherm by raising the thermal gradient and by introducing hot asthenospheric material from below to replace attenuated lithosphere. The thermal evolution of the lithosphere as it stretches depends principally on the relative rates of advection of heat into the lithosphere by upwelling of asthenosphere and diffusive loss of heat through increased surface heat flow, while thermal diffusion dominates after the end of stretching.

A logical extension of thermal models of lithospheric extension is the consideration of dynamic effects of rheology on the deformation. Earth materials generally have temperature-dependent material properties, so the thermal evolution and the mechanical evolution of stretching lithosphere are strongly coupled. In general, diffusion of heat during stretching results in the cooling of individual horizons in the lithosphere, as they are brought close to the earth's surface; with continued stretching this cooling may cause the vertically-averaged strength of the lithosphere to increase (England, 1983). This suggests that there may be a limit to the extensional strain attainable which would depend primarily on the magnitude of the driving stresses, the rate of deformation, and the degree of temperature dependence of the rheology (Houseman and England, 1986a; Sonder et al., 1987).

The calculations summarized above all considered the evolution of a single vertical column of lithosphere, and for simplicity, consideration was not given to the thermal and mechanical evolution, in three dimensions, of extending continental lithosphere or the effects thereon of a temperature-dependent rheology. This paper represents a preliminary investigation of the effects of such a rheology on the three-dimensional deformation of the continents in an extensional environment. We use a thin viscous sheet model (Bird and Piper, 1980; Vilotte et al., 1982, 1986; England and McKenzie, 1982, 1983) and treat the lithosphere as a continuum with vertically averaged properties. We first present general results of the calculations that illustrate the coupling between the thermal and mechanical behavior of the thin sheet, and we identify the phenomena that arise due to the inclusion of the temperature dependence.

The most important results presented in this paper concern the distribution of strains and strain rates. Calculations that include a temperature-dependent rheology result in a separation of the loci of maximum strain and maximum strain rate. The separation occurs as a result of increasing mechanical strength in thinned areas and begins after a time that can be approximated by the time required for thermal conduction to first affect temperatures in the uppermost mantle. Calculations with little or no temperature dependence do not produce this pattern of deformation. The results are compared with observations from the Aegean that indicate that, while the maximum Neogene extensional strain occurred in the southern Aegean north of Crete (Angelier et al., 1982), the maximum present-day strain rates are found in the northern Aegean. The consistency of the results of calculations with the observations allows us to propose a simple mechanism by which this deformation pattern may have been produced.

2. Choice of rheology

The thin viscous sheet model used in this paper requires the use of a vertically averaged rheology, and the choice of such a rheology, which is also to include temperature dependence, is of primary importance to the results discussed below. Laboratory experiments on olivine (e.g. Goetze, 1978) suggest that much of the long-term strength of the continental lithosphere may reside in the uppermost mantle (see Brace and Kohlstedt, 1980). Therefore, we are motivated to choose a temperature-dependent rheology based on olivine, and will neglect the strength of the crust. Although this is necessarily an approximation to the behavior of geological materials over the range of temperatures, pressures, strain rates, and compositions relevant to continental deformation, the adoption of a more realistic, but more complicated, rheology is unwarranted at this stage. Use of the simple rheology based on the physical properties of olivine avoids the need to introduce extra parameters describing the dependence of the strength of the crust on temperature and, especially, the nature of the poorly understood mid-crustal transition from frictional sliding to creeping flow.

The laboratory results for olivine suggest an empirical creep law of the form

$$\dot{\epsilon} = A \exp\left(\frac{-Q}{RT}\right) (\sigma_1 - \sigma_3)^n \quad (1)$$

(e.g. Goetze, 1978) for differential stress $\sigma_1 - \sigma_3$ less than 200 MPa. Q is the activation energy, R is the gas constant, T is absolute temperature, $\dot{\epsilon}$ is strain rate, and A is a constant. The stress exponent n typically has a value of about 3. Generalizing in terms of tensor components of strain rate and deviatoric stress (τ), and writing as a vertical average, Eq. 1 becomes

$$\tau_{ij} = B \dot{E}^{\left(\frac{1}{n}-1\right)} \dot{\epsilon}_{ij} \quad (2)$$

where \dot{E} is the second invariant of the strain rate tensor, equal to $(\dot{\epsilon}_{ij} \dot{\epsilon}_{ij})^{1/2}$

(with summation over repeated subscripts), and τ_{ij} and $\dot{\epsilon}_{ij}$ represent vertically averaged quantities. B includes the temperature dependence and will be referred to below as the strength of the lithosphere:

$$B = C \int_{z_M}^{z_L} \exp \left[\frac{Q}{nRT(z)} \right] dz \quad (3)$$

where z_L and z_M are the depths to the base of the lithosphere and the Moho, respectively, and C is a constant.

In a later section we present results of calculations of Moho temperature, T_M . The significance of the Moho temperature is that it is a convenient indicator of lithospheric strength for continental lithosphere whose deformation is governed by a power law such as Eq. 2 (England, 1983; Sonder and England, 1986). This may be seen by considering an approximation to Eq. 3. For a constant thermal gradient γ , the integral in Eq. 3 may be evaluated:

$$B \approx C \frac{nRT_M^2}{Q\gamma} \exp \left(\frac{Q}{nRT_M} \right) \quad (4)$$

England (1983). Thus, the strength increases sharply with decreasing Moho temperature. To a much lesser extent, B depends on the thermal gradient, γ ; this is important if thermal diffusion is small compared with advection of heat, when deformation may alter the thermal gradient without appreciably changing the Moho temperature.

A second important parameter is Q/RT_L , where T_L is a reference temperature, here taken as the temperature at the base of the lithosphere. For the magnitude of Q suggested by laboratory experiments on olivine, Q/RT_L falls in the range 30–50, if we assume that T_L is around 1400 °C.

3. Duration of extension: simple analytic model

England (1983) showed that, during continental extension, decreasing temperatures in strength-controlling regions of the lithosphere (e.g. the uppermost mantle) can cause the vertically-averaged strength of the lithosphere to increase sharply. For a range of conditions of driving stress, strain rate, and thermal state, this strength increase can be sufficient to limit further extension (e.g., Houseman and England, 1986a).

If extension of the lithosphere were to occur instantaneously and homogeneously by a factor β , there would be a discontinuity in the slope of the geotherm at the base of the lithosphere (depth z_L / β), which would relax with time, resulting in cooling of the lithosphere (see Figure 1) (McKenzie, 1978a). The exponential dependence of strength B in Eq. 4 on the temperature at the Moho means that rather small changes in Moho temperature produce large changes in B (England, 1983; Houseman and England, 1986a). Therefore, to a good approximation we can neglect changes in temperature except as they appear in this exponential term and write that the change in Moho temperature $\Delta T(b)$ required to produce a change in lithospheric strength by a factor b is

$$\Delta T(b) \approx \frac{nRT_M}{Q} \ln(b) \quad (5)$$

Evaluation of Eq. 5 for values of the parameters believed to be appropriate to the continental lithosphere ($Q \approx 5 \times 10^2 \text{ kJ mol}^{-1}$; $n = 3$; $T_M \approx 800 \text{ K}$) shows that a ten-fold increase in lithospheric strength ($b = 10$) results from a drop of a few percent in Moho temperature, so the approximations in going from Eq. 4 to Eq. 5 are not severe.

Because we are concerned with small temperature changes at the Moho, and hence with times small compared with the time for thermal relaxation of the lithosphere, the time for these temperature changes is governed by the distance

$(z_L - z_M)/\beta$ from the Moho to the "knee" in the thermal profile (Figure 1). Neglecting geometrical factors, the change in Moho temperature may be written:

$$\Delta T \approx T_L \operatorname{erfc} \left[\frac{(z_L - z_M)/\beta}{2\sqrt{\kappa t}} \right] \quad (6)$$

where κ is the thermal diffusivity. Eliminating ΔT between Eqs. 5 and 6 gives an expression for the length of time required to increase the strength of the lithosphere by a factor b :

$$\frac{(z_L - z_M)/\beta}{2\sqrt{\kappa t}} \approx \operatorname{erfc}^{-1} \left[\frac{nRT_L}{Q} \left(\frac{T_M}{T_L} \right)^2 \ln(b) \right] \quad (7)$$

Evaluating Eq. 7 with $Q \approx 5 \times 10^5 \text{ J mol}^{-1} \text{ K}^{-1}$, $n = 3$, and $T_L = 1600 \text{ K}$, and a Moho temperature approximately half that of the base of the lithosphere gives the result that an increase in lithospheric strength by a factor of ten ($b = 10$) is obtained at a time t_c , where

$$t_c \approx \frac{(z_L - z_M)^2 / \beta^2}{8 \kappa} \quad (8)$$

Although this discussion relates to an instantaneously stretched lithosphere, it has the advantages of showing that the timescale for the evolution of strength of the lithosphere is generally short compared with the thermal time constant of the lithosphere as a whole, and of relating the timescale to the rheological parameters. If, instead, we consider extension that occurs over a finite time interval, we may suggest a modification to the previous discussion. For simplicity, assume that the strain rate $\dot{\epsilon}$ is a constant equal to $\dot{\epsilon}_0$; then

$$\beta = \exp(\dot{\epsilon}_0 t) \quad (9)$$

and

$$t_c \approx \frac{z_L^2}{8\kappa} \left[1 - z_M/z_l \right]^2 e^{-2\dot{\epsilon}_0 t_c} \quad (10)$$

The form of Eq. 10 is a natural one for considering thermal diffusion alone, but a second timescale is involved when the mechanical problem is considered. In the calculations below, the extensional strain rates – at least before the development of rheological contrasts of the kind just discussed – depend on the characteristic horizontal length of the extensional boundary and on its speed (see England et al., 1985). For example, in the configuration we adopt here, strain rates near the extensional boundary are about v_0/w , where v_0 is the velocity of the boundary and w is the width of the moving boundary (see Figure 3). In the mechanical calculations we use a dimensionless time t' given by

$$t' = \frac{v_0 t}{D}$$

where D is the width of the solution domain. Eq. 10 may be written in dimensionless form as

$$t_c' \approx \frac{Pe z_L'^2}{8} \left[1 - z_M' / z_L' \right]^2 e^{-2\dot{\epsilon}' t_c'} \quad (11)$$

where lengths are made non-dimensional by $z' = z/D$, and strain rates by $\dot{\epsilon}' = \dot{\epsilon}D/v_0$. The Peclet number, Pe , in Eq. 11 is given by

$$Pe = \frac{v_0 D}{\kappa} \quad (12)$$

It is this parameter that determines the relative importance of thermal diffusion and advection in the calculations below. At low Peclet number, thermal diffusion will influence the temperature structure, and hence the strength, before appreciable strain has occurred, whereas at high Peclet number, large strains may occur essentially isothermally.

Figure 2 shows solutions of Eq. 10 for values of 2, $\sqrt{2}$, and 1 for the right hand side of Eq. 7, corresponding to values of 16, 8, and 4 for the constant in the denominator of Eq. 10. The right hand side of Eq. 7 can be easily evaluated for a given choice of values for the parameters. The three values of Q/RT_L used in this paper are 50, 25, and 12.5 (Table 1). These, with $b = 10$ and the values of T_M and T_L shown in Table 2 give values, respectively, of 1.5, 1.3, and 1.1 for the right hand side of Eq. 7; solutions of Eq. 10 using these values are illustrated in Figure 8, and compared with the equivalent times determined from three-dimensional calculations in which the changes in rheology explicitly affect the strain rate field.

4. Three-dimensional calculations of extension with a temperature-dependent rheology

4.1. Description of model

Following England and McKenzie (1982, 1983), we approximate the deformation of continental lithosphere by the deformation of a thin sheet of incompressible viscous fluid that overlies an inviscid half-space. Because the horizontal dimensions of the sheet are much greater than the vertical dimension, and shear stresses are assumed to be zero on the top and bottom of the sheet, the deformation can be approximated by neglecting vertical gradients of horizontal velocity components. This allows the deformation of the sheet to be expressed in terms of vertical averages of strain rate, deviatoric stress, and rheology. The sheet is also assumed to be in isostatic equilibrium.

The problem consists of two parts, mechanical and thermal, that are coupled through the temperature dependence of the rheology. The formulation of the equations of motion, which follows England and McKenzie (1982, 1983), and of

the equation governing heat transfer are summarized in the Appendix. Solution of the equations is accomplished using a Lagrangean finite element scheme (Houseman and England, 1986b), also summarized briefly in the Appendix.

4.2. Boundary and initial conditions and parameter ranges

Figure 3 shows the boundary conditions used in the calculations. The solution domain is initially a 2×1 rectangular box. Three sides ($x' = -1$, $x' = 1$, and $y' = 1$) are rigid ($u' = 0$, $v' = 0$). On the boundary initially at $y' = 0$, the tangential velocity is zero; the normal velocity is specified such that part of the boundary moves outward with respect to the rest of the box, resulting in horizontal stretching and vertical thinning of the fluid near the boundary.

Thermal boundary conditions are $T' = 0$ and $T' = 1$ on the upper and lower surfaces, respectively, of the fluid. Initial conditions are uniform thickness of crust and lithosphere and a constant vertical temperature gradient at all points (x, y) in the box. Hence, initially, there are no horizontal gradients of layer thickness or temperature.

Calculations were carried out using the values of the dimensionalizing constants in Table 1. For a given set of boundary conditions, there are four dimensionless parameters that define the solution space of the thin viscous sheet model with temperature-dependent rheology. Three of them have been introduced earlier (Q/RT_L , Pe , and n), and describe, respectively, the degree of temperature dependence of the rheology, the relative rates of advection and diffusion of heat, and the nonlinearity of the stress dependence of the rheology. Apparent values of these parameters appropriate to the deformation of the continents are discussed more fully in the Appendix, and are listed in Table 2. We only consider deformation with $n = 3$ because this is the value appropriate to the power law creep regime -- in which the uppermost mantle is believed to be at geologically

relevant strain rates. The remaining dimensionless parameter is the Argand number (Ar ; England and McKenzie, 1982; also see Section 4.3.4), which expresses the degree to which buoyancy forces due to horizontal density gradients influence the deformation.

4.3. Results

We first present results with $Ar = 0$, in order to understand those aspects of the deformation that depend on the temperature dependence of the rheology. Calculations are presented later (Section 4.3.4) that have non-zero Argand numbers, so that the modifying effects of buoyancy forces on the deformation can be identified.

4.3.1. Time evolution of selected nodes

Figure 4 shows the time evolution of Moho temperature (T_M), strength (B), vertical strain rate ($\dot{\epsilon}_{zz}$), and strain (β) for five nodes of the finite element mesh. For this experiment, $Pe = 300$, $Q/RT_L = 50$, $n = 3$, and $Ar = 0$. Because of the Lagrangean finite element formulation used to solve the equations of motion, the mesh deforms with the fluid, so that by tracking these five nodes through time, we are tracking the history of five individual fluid parcels.

At first, Moho temperatures and strengths are uniform over the entire solution domain, so the distribution of strain rates is governed entirely by the boundary conditions and the value of the power law exponent (see England et al., 1985). The region of greatest extensional strain rate is located on the boundary of the mesh, and the rate of extension decays with distance from the boundary. Extension proceeds for approximately 0.1 dimensionless time unit without a large change in Moho temperature (Fig. 4a). There is a slight (20%) decrease in strength (Fig. 4b), most apparent for the nodes closest to the extensional

boundary; this decrease is attributed to the increased thermal gradients resulting from the lithospheric thinning (see Eq. 4). Weaker areas, those closest to the boundary, concentrate the strain, so strain rates increase in those regions and decrease slightly elsewhere (Fig. 4c).

With continuing extension, by $t' = 0.1$ sufficient time has elapsed that the temperature at the Moho begins to drop (Fig. 4a). The temperature decrease is largest for nodes closer to the boundary, where there has been more extension. At the same time the strength begins to increase. For nodes 1, 2, and 3, the strength increase results in a sudden and sharp decrease in the rate of extension. Extension begins to be taken up in regions farther from the boundary (e.g. nodes 4 and 5) where the strength is less. By $t' = 0.25$, the region of maximum rate of extension is well within the interior of the fluid and the rate of extension on the boundary is approximately 10% of its original rate.

As time proceeds, the strength also increases for nodes located away from the boundary (nodes 4 and 5), so strain rates peak there at $t \simeq 0.2$. The distribution of strain rates becomes spatially more uniform as the high strength of many nodes causes quasi-rigid behavior of the most highly extended parts of the fluid. By the end of the experiment, the strain rates for all 5 nodes are close to zero (Fig. 4c) and little additional strain is accumulating in the region illustrated in Fig. 4 close to the boundary (see Fig. 4d, in which β has levelled off at values between 1.4 and 1.6). Almost all the deformation is being taken up further into the interior of the fluid.

4.3.2. Strain rates

In Figure 5 the horizontal distribution of vertical strain rate as a function of time is shown for the experiment of Figure 4 ($Pe = 300$, $Q/RT_L = 50$, $n = 3$, and $Ar = 0$). At first, extensional strain rates are greatest near the

boundary of the fluid; the form of the boundary condition also concentrates strain rates near the taper in the boundary velocity (Fig. 3). The early concentration of high strain rates near the boundary due to the slight strength decrease is plainly seen as a decrease in the spacing of contours. By $t' = 0.2$ the pattern of strain rate distribution is beginning to change. The rate of extension begins to drop, initially on the boundary where the strains are greatest, and the region with $|\dot{\epsilon}_{zz}| > 0.8$ begins to broaden and move towards the interior of the fluid. It is well away from the boundary by $t' = 0.4$, the end of the calculation.

Figure 6 illustrates the influence of the choice of Peclet number and Q/RT_L on the distribution with time of the strain rate field. The plots shown are for $t' = 0.4$; in all cases the Argand number is 0.

The degree to which the distribution of strain rates is controlled by the temperature dependence (Q/RT_L) is clearly seen. When Q/RT_L is large (i.e. 50), high strain rates are confined to a region that moves progressively towards the interior of the fluid. For the intermediate value of Q/RT_L (25), this separation is less pronounced or is absent. If it is present, the distance from the boundary of the locus of high strain rate is less than that for the equivalent experiment with larger Q/RT_L .

When Q/RT_L is small, extensional strain rates are generally largest on the boundary of the box. In these instances, the change in Moho temperature required to affect the vertically averaged strength (see Eq. 4) is sufficiently large that it is not attained until near the end of the experiment (e.g. $Pe = 300$), or not attained at all (e.g., $Pe = 1000$ or 3000).

The effect of lithospheric attenuation on the vertically averaged strength of the lithosphere and on the course of deformation is most clearly seen in the plots in which $Q/RT_L = 12.5$ and the Peclet number is large; in this case a decrease in Moho temperature does not increase the strength. However, weakening of the

lithosphere due to thinning (see Eq. 3) causes strain to be concentrated in a small region along the boundary. Further extension there causes additional weakening; this positive feedback can be considered to be a kind of viscous stretching instability, which for larger values of Q/RT_L (> 25) is stabilized by the effect of temperature decreases brought about by thermal diffusion.

Since the Peclet number is a measure of the relative rates of advection and diffusion of heat, it controls the timing of strength changes. Thus, it will affect when the locus of high strain rates begins to move away from the boundary, and how fast such a region will shift towards the interior of the fluid. This can also be seen in Figure 6. Experiments with small Peclet number, which have a fast rate of thermal diffusion relative to advection, show strain rate maxima that have had longer to develop and so are broader in area, shallower, and further from the boundary than experiments with higher Peclet numbers. In fact, for $Pe = 300$ and $Q/RT_L = 25$ or 50 , the strain rate maximum has become so broad that it is not distinguishable with the contour interval chosen.

More quantitatively, an understanding of the timing of strength changes can be obtained through a comparison of the results of the numerical calculation with the critical times predicted by the simple model of Section 3. The curves in Fig. 7 are the critical times calculated as a function of strain rate with the right hand side of Eq. 7 evaluated for the parameters of Table 2, as discussed in Section 3. The relevant critical dimensionless time in the numerical experiments is chosen to be the time at which the strength B/B_0 (Eq. 4) begins to increase at node 1 of the mesh (see Fig. 3 for node locations). The dimensionless strain rate in each case is taken to be the starting value at node 1 (≈ 2.2 —see Fig. 4). These dimensionless times and strain rates are made dimensional for the purposes of plotting on Fig. 7 by multiplication or division by the appropriate timescale, which is

$$\frac{D^2}{\kappa Pe} \text{ (see Section 3).}$$

The agreement between the critical times determined from the full thermo-mechanical calculations and those calculated from Eq. 10 is close enough to warrant the use of Eq. 10 as a convenient rule-of-thumb.

4.3.3. Vertical strain

Figure 8 shows the calculated distribution of vertical strains (β) at a dimensionless time of 0.4 for experiments with different values of Pe and Q/RT_L . Substantial crustal thinning has occurred by this time for all experiments, but the distribution differs, owing to the effects of the temperature dependent rheology.

Because of the migration of the locus of high strain rates away from the boundary (see Figs. 4 and 5) experiments with low Peclet numbers (in which rapid thermal diffusion has produced substantial horizontal differences in strength) tend to produce broad regions of moderately thinned crust. For example, when $Pe = 300$, strains are less than $\beta = 2.5$, except along the tapered part of the boundary. Conversely, when the Peclet number is large, the strain along the boundary exceeds $\beta = 4$ in all cases shown and the distribution is similar to that produced when the rheology is independent of temperature ($Q/RT_L = 0$). To a lesser extent, these differences are also evident as a function of Q/RT_L . A highly temperature dependent rheology results in more uniformly distributed extension than one with little or no temperature dependence.

4.3.4. Buoyancy forces

In the calculations presented so far, we have not considered the effects of buoyancy forces arising from horizontal variations in density. However, it is clear that such forces can be important whenever deformation produces lateral contrasts in crustal or lithospheric thickness (e.g. Artyushkov, 1973; Fleitout and

Froidevaux, 1982; England and McKenzie, 1982; LePichon, 1983; Sonder et al., 1987). During continental extension, thinning of the crust and attendant replacement by denser mantle gives rise to buoyancy forces that act to decrease the net potential energy available to drive continued extension. In contrast, if the mantle lithosphere also thins, the replacement of mantle material with less dense asthenosphere has the opposite effect of tending to increase the extensional stress (see Le Pichon, 1983, Artyushkov, 1973). The net buoyancy force will be the sum of these two effects, and depends on the densities of crust, mantle, and asthenosphere, and the amount and vertical distribution of thinning.

In terms of the thin viscous sheet model, the sensitivity of the lithosphere to such buoyancy forces is described by the Argand number (England and McKenzie, 1982; also see the Appendix). $Ar > 0$ corresponds to the situation in which buoyancy forces arising from horizontal variations in crustal thickness are large and opposite in sign to viscous forces driving the deformation. Such lithosphere can be considered too weak to support large gradients in crustal and lithospheric thickness. On the other hand, $Ar < 0$ represents the state in which buoyancy forces resulting from extension act to augment other extensional forces. Finally, $Ar = 0$ implies the state in which buoyancy forces do not influence the deformation, neither damping nor amplifying the extension.

Figure 9a shows the influence of the Argand number on the strain fields; experiments are shown for $Ar = -3, 0, \text{ and } 3$, with $Q/RT_L = 0$. Since when $Ar > 0$, buoyancy forces due to crustal thickness gradients result in pressure gradients directed away from areas of thicker crust and towards areas of thinner crust, less crustal thinning results than when $Ar = 0$. Conversely, when $Ar < 0$, the buoyancy forces act to localize deformation at previously thinned areas, so that deformation is confined to a smaller area in which strains are greater than when $Ar \geq 0$. For example, when $Ar = -3$, the area with $\beta > 4$

includes approximately 2/3 of the total area with $\beta > 1.5$, but only 1/3 when $Ar = 0$, and is confined to the vicinity of the taper in the boundary condition when $Ar > 0$.

When $Ar < 0$ the deformation can be considered to be unstable, in the sense that it localizes around previously deformed regions. However, when a temperature dependent rheology is also included, the increase in strength of previously strained areas stabilizes the deformation, as shown in Figure 9b, for experiments with $Q/RT_L = 50$, and $Ar = -3, 0$, and 3 . Although horizontal gradients in vertical strain are still greater when $Ar < 0$ (or less when $Ar > 0$) than when $Ar = 0$, in all cases the extensional strain and the horizontal gradients in strain at any point are less than when $Q/RT_L = 0$.

5. Comparison with the Aegean

We have presented general results for the extensional deformation of a thin viscous sheet with a temperature- and stress-dependent rheology. In this section we test the applicability of the model to continental extension by quantitatively comparing results of the calculations with observations of recent and active deformation in the Aegean region.

Aegean extension began in the middle to late Miocene (13-10 Ma ago) (Le Pichon and Angelier, 1979) or possibly as late as 6 Ma ago (McKenzie, 1978b). Total extension of up to 100% is believed to have occurred in a north-south direction (McKenzie, 1978b), with the greatest extensional strain located in the southern Aegean, north of Crete (e.g., Angelier et al., 1982). The region that has experienced extension (see Figure 11) is roughly 5×10^5 km² in area (Le Pichon, 1983) and is bounded to the south by the Hellenic trench, and to the west by thrusting and compression in Albania and northwestern Greece. Extensional deformation dies out north of 42 °N in Yugoslavia, Bulgaria and northern

Greece, and east of 31° E in Turkey (see Angelier et al., 1982).

If the scale, D , is chosen to be 1000 km then the size of the extensional boundary in the calculations corresponds approximately to that of the Hellenic trench, and its displacement by 400 km at a dimensionless time of 0.4 is in rough agreement with the estimates quoted above for net extension in the Aegean. With this scaling, the range of Peclet numbers (300, 1000, 3000) investigated in the calculations of Section 4 correspond to magnitudes of 10, 30, and 100 mm yr⁻¹ for the outward velocity of the boundary. The dimensionless time of 0.4, at which displacement of the extensional boundary reaches 400 km, corresponds to 40 Ma ($Pe = 300$), 13 Ma ($Pe = 1000$), and 4 Ma ($Pe = 3000$). The longest of these times is greater than that believed to be available for the Aegean extension, but the two shorter times cover the range of estimates given by Le Pichon and Angelier (1979) and McKenzie (1978b) for the duration of the extension.

The values of Q/RT_L of 50, 25, and 12.5 correspond to activation energies for creep of 580, 290, and 150 kJ mol⁻¹.

For convenience we shall refer to regions in the solution domain in terms of geographical directions---north, south, east, and west---with the $+y$ -direction being north (see Figure 3). We emphasize that the geometry and boundary conditions shown in Figure 3 were chosen for their simplicity, and not to simulate in detail the kinematics of the Aegean. Hence we have not attempted to reproduce the exact geometry of the region, nor have we included any effects related to right lateral strike-slip motion along the North Anatolian fault.

5.1. Extensional strain

The pre-Miocene geology of the Aegean is similar to that of unextended regions in mainland Greece and Turkey (see summary by Horvath and Berckheimer, 1982). Therefore, rough estimates of the total extension in the Aegean can

be made by comparing present-day crustal thicknesses with those of Greece and Turkey, about 40-50 km (Makris, 1975; Makris and Veis, 1977). Seismic refraction experiments have shown that the crustal thickness is 30-34 km under Crete, approximately 26 km beneath Amorgos in the central Aegean, and about 32 km under Evia, east of the Peloponnese (Makris and Veis, 1977). This suggests thinning by factors of approximately 1.4, 1.7, and 1.4, respectively.

Post-Miocene extensional strain in the Aegean has also been determined using plate motion data and subsidence data and is consistent with the rough estimates given above. From slip vectors of earthquakes located along the Hellenic trench, relative rotation rates of the European plate, African plate, and Aegean region and constraints imposed by fault trends and offsets, Le Pichon and Angelier (1979) estimated displacements along the boundaries of the extending region; the displacements were interpolated to give strains in the interior of the region. In the southern Aegean, average subsidence data for rectangular regions 2100-3800 km² in area were used in conjunction with a simple uniform stretching model (McKenzie, 1978a) to obtain more detailed estimates of strain (Angelier et al., 1982).

Uncertainties in the reconstructions are difficult to determine. Some indication may be afforded by the calculated uncertainty in the strain averaged over the entire southern Aegean of $\beta = 1.65 \pm 0.25$ given by Angelier et al (1982). However, it is more likely that strains are underestimated than overestimated. Determining the amount of extension from the ratio of the inferred pre-extensional crustal thickness to the present-day crustal thickness does not take into account additions to crustal thickness by mantle-derived magmatism, and determinations of strain that rely on offsets across normal faults will underestimate extension if the faults are listric.

To summarize the Aegean strain data, the region affected by extensional strain ($\beta \geq 1.1$) is approximately 700 km by 700 km in area. Maximum strain of $\beta = 1.8$ occurs in the Sea of Crete; south of this a sharp decrease in strain (from $\beta = 1.8$ to 1.4) occurs over a distance about 100 km. Strains decrease gradually to the north of the Sea of Crete; the $\beta = 1.1$ contour is 400-500 km distant from the zone of maximum strain. Strains greater than $\beta = 1.5$ are confined to the southern Aegean, and occur in an area approximately 250 km (N-S) by 500 km (E-W).

To compare calculated strains (Fig. 8) with observed strains (Fig. 10), we consider calculated strains near the center of the extending region (i.e., along $x = 0$), since the large strains on the east and west margins of the area are numerical artefacts that occur due to the taper used in the boundary conditions. In all calculations, the portions of the fluid with $\beta > 1.5$ are within 450 km of the southern boundary, and in the case of the experiment with $Pe = 300$, $Q/RT_L = 50$, and $Ar = 0$, the $\beta = 1.5$ contour is about 250 km from the boundary. Maximum calculated strains along $x' = 0$ range from less than 2.0 at low Peclet number and high Q/RT_L to considerably above 4.0 when the influence of temperature changes on the rheology is small (e.g. when $Pe = 3000$). None of the experimental results shows the sharp southwards decrease in β from 1.8 to 1.4 that occurs in the southern Aegean. The combination of parameters that exhibit a region with $\beta < 1.1$ comparable in extent to that of the Aegean and maximum extensional strains $\beta \leq 2.5$ is $Pe \approx 1000$, $Q/RT_L \approx 50$ (c.f. Fig. 8).

5.1.1. Strain rates

A striking feature of the strain field in the Aegean is that while the greatest extensional strain is in the southernmost part of the region (Angelier et al., 1979; see Fig. 10, this paper) the most active region at present is some 300 km north of the trench. This is illustrated in Figure 11a, which shows the distribution of normal and strike-slip earthquakes in the Aegean region for this century (Jackson and McKenzie, 1988), and Figure 11b, which shows the shallow seismicity of all types for the region.

Figure 12a shows the cumulative seismic moment release in the earthquakes of Fig. 11a, plotted as a function of distance north of 35°N (the approximate southern limit of extensional deformation). Approximately 80% of the moment has been released in the region 400 km to 800 km north of the trench. As Figure 12a and the analysis of Jackson and McKenzie (1988) shows, the average strain tensor expressed in this seismicity is nearly biaxial with north-south extension and vertical thinning; thus the profile of moment release in Fig. 12a may equally be regarded as a profile of (seismically expressed) northward displacement of the north of the region with respect to the south. Jackson and McKenzie (1988) estimate that the moment release shown in Fig. 12a corresponds to a displacement of 2.4 to 8 m over the interval 1909-1981 or an average relative velocity of 33 to 113 mm yr^{-1} .

The observed profile of cumulative seismic moment release, or north-south displacement, may be compared with the velocity fields calculated in the experiments discussed above; this is done in Figures 13b, c, d. As in the case of the total strain, the quantity of interest is rather more sensitive to the Peclet number than to the value of Q/RT_L . All calculations with $Pe = 3000$ show a concentration of strain rate towards the southern boundary, irrespective of the activation energy shown. However, for each activation energy, a calculation with a

lower Peclet number can be found that exhibits slower strain rates in the southern 200-300 km of the extended region in the fashion shown by the seismic data; for $Q/RT_L = 50$, this Peclet number is about 1000 (Fig. 12b), for $Q/RT_L = 25$, it is between 1000 and 300 (Fig. 12c), and for $Q/RT_L = 12.5$, it is about 300 (Fig. 12d). The best agreement between the normalized moment release curves and the calculated velocity curves is for $Q/RT_L \approx 50$, $Pe \approx 1000$.

5.2. Finite rotations and paleomagnetic data

Figure 12 shows paleomagnetically determined rotations of Oligocene and younger rocks in the Aegean. Clockwise rotations of up to 25° are found for upper Miocene rocks on the Ionian islands of Kephallinia, Corfu, and Zakynthos (Laj et al., 1982). In the Epirus-Akarnania region of northwestern Greece, rotations of Eocene and Oligocene rocks range from $35-50^\circ$, clockwise (Horner and Freeman, 1983; Kissel et al., 1985). Clockwise rotations tend to be smaller eastwards: about 25° on the Chalkidiki peninsula (Kondopoulou and Westphal, 1986), 26° on Skyros, 48° on Evia (Kissel et al., 1986a), and 6° on Lesbos (Kissel et al., 1986b). No significant rotation has occurred on Crete and Rhodes since the upper Miocene (Valente et al., 1982; Laj et al., 1982), in the Volos region in Greece since the middle Pliocene, or in Thrace since the lower Oligocene (Kissel et al., 1986a). Preliminary work on Miocene rocks in the Izmir area of western Turkey suggests 29° of counterclockwise rotation (Kissel et al., 1986b).

Calculated finite rotations at $t' = 0.4$ are shown in Figure 13 for several numerical experiments. The results are not substantially different from each other, indicating that the finite rotations do not depend on the temperature dependence of the rheology, but are controlled mainly by the boundary conditions; the rotations of the material lines that make up the tapers on the

boundary account for most of the calculated rotations in the interior, with additional rotation about vertical axes arising from the shear component of deformation near these tapers.

The calculated results agree with the paleomagnetic data: rotations are clockwise in the west, decrease to zero in the center of the extending region, and are counterclockwise in the east. However, the paleomagnetic data do not constrain parameter ranges in the manner that the strain and strain rate fields do (Sections 5.1, 5.2).

5.3. Summary of implications for the Aegean

The combination of parameters that provide the closest agreement between the observed and calculated strains and strain rates is a Peclet number of around 1000 and Q/RT_L of 25 to 50. With the scaling of Table 2, the value of 1000 for the Peclet number corresponds to an outward velocity of 32 mm yr^{-1} for the southern boundary, and the duration of the motion that produces displacement of this boundary by 400 km is 12.5 Ma.

McKenzie (1987b) estimates 70 mm yr^{-1} for the velocity of southernmost Aegea with respect to Eurasia, and Jackson and McKenzie (1988) estimate values of $30\text{-}113 \text{ mm yr}^{-1}$ from the seismic moment release in the region. The duration of 12.5 Ma for the extension is comparable with Le Pichon and Angelier's (1979) estimate of $10\text{-}13 \text{ Ma}$ and about twice McKenzie's (1978b). Little significance should be attached, however, to a factor of two in these comparisons, owing to uncertainties in the observations and the simple configuration of the calculations.

The average strain rate implied for the Aegean region from McKenzie's (1978b) or Le Pichon and Angelier's (1979) estimates of the amount and duration of strain is in the range $1 \text{ to } 3 \times 10^{-15} \text{ s}^{-1}$. The scaling arguments of Section 3 suggest that this is within the range of conditions in which thermal diffusion will

limit extension, and the rule-of-thumb illustrated in Fig. 2 shows that, for a lithosphere whose rheology is determined by the creep of silicates, the maximum achievable extensional strain may be less than about $\beta = 2$. The comparisons of this section support the idea that the low strain rates and high strain in the southernmost Aegean are the result of this mechanism.

6. Implications for stretching instabilities

Recently, several workers (Fletcher and Hallet, 1983; Zuber and Parmentier, 1986; Zuber et al., 1986) have studied lithospheric extension in terms of the mechanics of necking instabilities that develop in media consisting of horizontal layers with contrasting rheologies. In these models, the instabilities, once formed, grow exponentially with rates that depend on the strength contrasts of layers and with wavelengths that depend on the relative thicknesses of the layers.

In this paper, we have identified two other phenomena that contribute to the instability of continental lithosphere during extension. First, the weakening of continental lithosphere in the early stages of extension (Fig. 4b), before there has been sufficient time for temperatures at or below the Moho to decrease, will tend to concentrate extension in previously thinned regions. Second, we have demonstrated that if buoyancy forces arising from horizontal density variations (Sec. 4.3.4) act to increase the force available to drive extension ($Ar < 0$), deformation will be concentrated in narrower zones.

However, the dominant effect of temperature dependence will be to stabilize continental extension. As the uppermost mantle temperatures decrease in stretched continental lithosphere, the strength will increase. It becomes more difficult to continue to extend already stretched lithosphere than to begin to extend unstretched lithosphere, and the growth of instabilities is highly damped.

7. Discussion and conclusions

We have used a thin viscous sheet model to investigate the influence of a temperature-dependent rheology on continental deformation in an extensional environment. During the early stages of extension, attenuation of the lithosphere causes the vertically-averaged strength of the lithosphere to decrease slightly, and strain is concentrated into the regions that have already strained the most (e. g. Fig. 6; Fig. 8). However, after a critical time (which can be estimated from the arguments given in Section 3), thermal diffusion lowers the temperature in the lithosphere and so increases its strength. This critical time depends on the relative rates of strain and thermal diffusion (described by the Peclet number) but is short compared with the thermal time constant of the lithosphere (Fig. 2). However, at high strain rates the extensional strains that are achieved before this critical time is reached are so great that it is reasonable to expect sea-floor spreading to begin. At lower strain rates, thermal diffusion can cause changes in strength at small extensional strains. These changes in strength cause the locus of maximum strain rate in a zone of extension to shift as much as a few hundred kilometers during the duration of extension; in general the location of the strain rate maximum will move from regions of high strain to regions of lower strain. If sufficient time elapses, the effect of the migration of loci of high strain rate is the creation of wide zones of moderate extensional strain, rather than smaller areas of greater extension. The transition between essentially isothermal extension which, if continued, would lead to seafloor spreading, and extension that is almost completely inhibited by strength increases due to thermal diffusion takes place between strain rates of 10^{-14} and 10^{-16} s^{-1} .

Buoyancy forces due to horizontal gradients in crustal or lithospheric thickness can modify the deformation. Depending on whether the buoyancy forces act to augment (i.e. $Ar < 0$) or diminish (e.g. $Ar > 0$) the viscous forces arising

from the imposed boundary velocity, they can increase or decrease, respectively, the total strain and strain gradient at points within the deforming fluid. However, when there is moderate or greater temperature dependence in the rheology ($Q/RT_L > 25$), the effect of buoyancy forces on the deformation is of secondary importance.

The Miocene-to recent extension of the Aegean region appears to have taken place at an average strain rate of 1 to $3 \times 10^{-15} \text{ s}^{-1}$. Extensional strains are greatest in the southern Aegean, approaching 100% extension, but present-day strain rates are concentrated in the northern Aegean. This spatial separation of the regions of maximum strain and maximum strain rate may be the consequence of the temperature dependent rheology of lithospheric materials. The comparisons between observations and calculations (Sections 5.1 and 5.2) reinforce this suggestion, and show that the present pattern of strain and strain rate in the Aegean are consistent with the deformation of lithosphere whose rheology is controlled by the properties of olivine determined by laboratory experiments (e.g. Goetze, 1978), subjected to an extensional boundary moving at 30-60 mm yr⁻¹.

In general, the effects of a temperature dependent rheology provide a mechanism for understanding why there can be spatial and temporal changes in the distribution of extension. This mechanism is a simple but inevitable consequence of the extension, and may reduce the need to invoke outside influences, such as changes in plate boundary forces, to explain observations of time- and space-varying continental extension.

Acknowledgements

We are grateful for support provided by NASA Crustal Dynamics Project grant NAS5-27229 and NSF grant EAR- 84-08352 (P.C.E.) and by an Exxon Teaching Fellowship (L.J.S.). L.J.S. also gratefully acknowledges support from a

Chaim Weizmann Postdoctoral Fellowship at Caltech and thanks Brad Hager for partial funding from NASA grant NAG5-842. We would also like to thank Greg Houseman, who wrote most of the finite element code use for the calculations.

L. J. S. also thanks the San Diego Supercomputer Center and Aron Kuppermann of Caltech for providing allocations of computer time on the San Diego Supercomputer Center's CRAY X-MP.

Division of Geological and Planetary Sciences contribution no. 4638.

Appendix: Physical and mathematical formulation

This formulation follows that of England and McKenzie (1983) and Houseman and England (1986a). The continental lithosphere is represented by a thin incompressible viscous fluid overlying an inviscid halfspace. Tractions are assumed to be zero on the top and bottom of the layer, which is in isostatic equilibrium. These assumptions allow the deformation of the sheet to be treated in terms of vertically averaged quantities. (Note that there is no consideration of the possibility of boudinage-type stretching instabilities of the lithosphere (see Zuber and Parmentier, 1986; Zuber et al., 1986). The deformation of the layer is governed by a vertically-averaged power law rheology (Eq. 2) where the temperature dependence is included in the term B (Eq. 4).

Given these assumptions, the equations of motion may be written in terms of horizontal components only:

$$\frac{\partial}{\partial x_i} \left[L \eta \left(\frac{\partial u_i}{\partial x_j} + \frac{\partial u_j}{\partial x_i} \right) \right] + \frac{\partial}{\partial x_i} \left[2L \eta \left(\frac{\partial u}{\partial x} + \frac{\partial v}{\partial y} \right) \right] = \frac{1}{2} \rho_c g (1 - \rho_c / \rho_m) \frac{\partial S^2}{\partial x_i} \quad (\text{A1})$$

where u and v are horizontal components of the velocity vector \mathbf{u} , L is the lithosphere thickness, ρ_c and ρ_m are respectively the densities of crust and

mantle, S is the crustal thickness, g is the acceleration due to gravity, and i and j take on the values 1 and 2 only. The vertical component of velocity is obtained through the incompressibility condition ($\nabla \cdot \mathbf{u} = 0$). The effective viscosity, η , is

$$\eta = \frac{1}{2} B \dot{E} \left(\frac{1}{n} - 1 \right) \quad (\text{A2})$$

The variation of temperature, T , with position and time is described by the heat transfer equation

$$\frac{\partial T}{\partial t} + \mathbf{u} \cdot \nabla T = \kappa \nabla^2 T \quad (\text{A3})$$

where κ is thermal diffusivity, and t is time. Heat production is neglected.

Equations (5.2) and (5.4) are made dimensionless by:

$$(x', y', z', L', S') = (x, y, z, L, S) / L_0$$

$$\mathbf{u}' = \mathbf{u} / v_0$$

$$t' = t v_0 / L_0$$

$$\eta' = \frac{2\eta}{B_0} \left(\frac{v_0}{L_0} \right)^{\left(\frac{1}{n} - 1 \right)}$$

$$T' = T / T_L \quad (\text{A4})$$

where B_0 is the value of B at $t = 0$. The dimensionless equations are:

$$\frac{\partial}{\partial x_j} \left[L \eta \left(\frac{\partial u_i}{\partial x_j} + \frac{\partial u_j}{\partial x_i} \right) \right] + \frac{\partial}{\partial x_i} \left[2L \eta \left(\frac{\partial u}{\partial x} + \frac{\partial v}{\partial y} \right) \right] =$$

$$Ar' \frac{\partial S'^2}{\partial x_i} \quad (\text{A5})$$

$$\frac{\partial T'}{\partial t'} + \mathbf{u}' \cdot \nabla T' = \frac{1}{Pe} \nabla'^2 T' \quad (\text{A6})$$

$$\eta = \dot{E} \left(\frac{1}{n} - 1 \right) (B / B_0) \quad (\text{A7})$$

where primes have been omitted. In order to be consistent with England and McKenzie (1982), who used a slightly different nondimensionalization, we define the Argand number, Ar , as

$$Ar = \frac{g \rho_c (1 - \rho_c / \rho_m) L_0}{B_0 (v_0 / L_0)^{\frac{1}{n}}} \quad (A8)$$

where L_0 is a characteristic vertical length scale, so that

$$Ar' = Ar \left(\frac{D}{L_0} \right)^{\left(\frac{1}{n} + 1 \right)} \quad (A9)$$

The Argand number may be thought of as the ratio of buoyancy forces arising from variations in crustal thickness of order L_0 to viscous forces required to deform the fluid at a reference strain rate v_0/L_0 . When $Ar = 0$, forces due to crustal thickness contrasts do not affect the flow, and as $Ar \rightarrow \infty$, the buoyancy forces dominate, making the fluid too weak to support large variations in crustal thickness, so that the deformation tends towards plane strain. As $Ar \rightarrow -\infty$, buoyancy forces also dominate, but they act in concert with the viscous forces so as to tend to enhance variations in crustal thickness.

Pe , the Peclet number, equals $\frac{v_0 D}{\kappa}$, and is a ratio of the time constant for thermal diffusion to the time constant for advection of heat.

For a given crustal and lithospheric thickness distribution, Equation (A5) is solved, subject to the specified velocity or stress boundary conditions, to give the horizontal velocities, u and v . The vertical strain rate is then obtained through the incompressibility condition, and in a Lagrangean coordinate frame, the rate at which crustal thickness, S , increases is given by:

$$\frac{1}{S} \frac{\partial S}{\partial t} = \dot{\epsilon}_{zz} = - \left(\frac{\partial u}{\partial x} + \frac{\partial v}{\partial y} \right) \quad (A10)$$

A useful measure of strain is the finite rotation, which may be thought of as the rotation of an infinitesimally small rigid disk embedded in the the deforming fluid (McKenzie and Jackson, 1983). It is obtained by integrating with respect to time half of the vertical component of the vorticity:

$$\theta = \int \dot{\theta} dt = \frac{1}{2} \int \left(\frac{\partial v}{\partial x} - \frac{\partial u}{\partial y} \right) dt \quad (\text{A11})$$

Numerical solution of governing equations

The equations describing the mechanical behavior of the sheet (Eq. A5) are solved using a finite element method (see Houseman and England, 1986a, Appendix B). The solution domain is divided into triangular elements, as shown in Figure 4. The Lagrangean coordinate system employed in the finite element approach permits considerable simplification of the calculation of the temperature field. In this reference frame the nodes travel with the fluid, so that there is no horizontal advection of heat relative to these nodes. In addition, horizontal gradients of temperature are small compared with vertical temperature gradients. Hence the dimensionless heat transfer equation reduces to:

$$\frac{\partial T}{\partial t} + \dot{\epsilon}_{zz} z \frac{\partial T}{\partial z} = \frac{1}{Pe} \frac{\partial^2 T}{\partial z^2} \quad (\text{A12})$$

At a given time t , the velocities in the thin layer are calculated from equation (A5) using the previously determined viscosities. The timestep Δt is then chosen so that the maximum strain in any element is less than or equal to 2.5%. Convergence of the velocity solution has been checked by running calculations with half the timestep or with approximately four times as many nodes. Once the timestep is chosen, a first order finite difference approximation to Eq. A10 allows the crustal thicknesses to be calculated at time $t + \Delta t$.

Temperatures are obtained by solving Eq. A6 using a Crank-Nicholson implicit finite difference scheme, which is uniformly stable. The finite difference grid spacing is $L_0/100$. Convergence of the temperature calculation was checked by comparison with solutions obtained using half the number of grid points.

After the new temperature field is obtained, the viscosity field at time $t + \Delta t$ is found by numerically integrating Eq. 3 and substituting into Eq. A7.

Figure captions

Figure 1: Sketch of thermal profiles of extended continental lithosphere, immediately after stretching (a) and a short time later (b). In the time interval between (a) and (b), thermal diffusion has lowered the Moho temperature by an amount ΔT , with a resultant increase in the strength of the lithosphere from B_0 to B (see Eq. 4). The relevant length scale for the diffusion is the distance $(z_L - z_M)/\beta$ between the base of the lithosphere and the base of the thinned crust. The original thicknesses of the lithosphere and crust are z_L and z_M .

Figure 2: Time for cooling to influence strength of extending lithosphere plotted against strain rate, calculated from Eq. 10. Numbers on the curves refer to the constant in the denominator in the right hand side of Eq. 10. This constant depends on a number of parameters (see Eq. 7) but the range illustrated here probably covers most of the values appropriate to the extension of continental lithosphere.

Figure 3: Finite element mesh and boundary conditions. Velocities are calculated at the vertices and midpoints of the sides of the triangular elements. The nodes labelled 1--5 are those referred to in Section 4.3.1 and in Figure 4. The y -component of velocity on $y = 0$ is: $v = -1.0$ for $|x| < 0.25 D$; $v = -\sin \left[\pi(0.4-x)/0.3 \right]$ for $0.25D \leq |x| \leq 0.4 D$; and $v = 0$ for $0.4 D < |x|$. Initial crustal thickness is $0.035 \times D$.

Figure 4: Moho temperature (a), strength (b), vertical strain rate (c), and vertical strain (d) for selected nodes, plotted as functions of time for an experiment with $Pe = 300$, $Q/RT_L = 50$, $Ar = 0$, $n = 3$. All units are dimensionless. Note that the vertical strain rate is plotted so that the absolute rate of

deformation increases upwards. Arrows on time axes correspond to the critical time for this run, calculated from Eq. 10.

Figure 5: Plots of the distribution of dimensionless vertical strain rate ($\dot{\epsilon}_{zz}$) at different times for the experiment shown in Figure 4 ($Pe = 300$, $Q/RT_L = 50$, $Ar = 0$, $n = 3$).

Figure 6: Dimensionless vertical strain rate ($\dot{\epsilon}_{zz}$) at $t' = 0.4$ for selected experiments.

Figure 7: Comparison between the rule-of-thumb calculation of the time at which cooling of the lithosphere has increased its strength appreciably (Eq. 10) and the times at which extension rates begin to decrease in the calculations of Figs. 6 and 8. Parameter values are those of Table 2. Numbers on the curves refer to values of Q/RT_L .

Figure 8: Extensional strain (β) at $t' = 0.4$ for selected experiments. The Argand number is zero in all plots. Except for the $\beta = 1.1$ contour, the contour interval is 0.5.

Figure 9: Extensional strain (β) at $t' = 0.4$ for selected experiments with varying Argand number. (a) $Q/RT_L = 0$, $Pe = 1000$. (b) $Q/RT_L = 50$, $Pe = 1000$.

Figure 10: Extensional strain estimated from observations in the Aegean (from Angelier et al., 1982). Contours indicate values of β , the ratio of the thickness of undeformed crust to that of stretched crust.

Figure 11: Seismic activity in the Aegean. (a) Focal mechanisms of extensional and strike-slip earthquakes in the Aegean in the interval 1909-1981 (Jackson and McKenzie, 1988). Larger mechanism represents the average of the individual mechanisms, each weighted by its scalar moment.

(b) Epicenters of earthquakes in the Aegean whose hypocenters are shallower than 35 km and whose body wave magnitudes are greater than 4.5, from the USGS catalog over the interval 1966-1984.

Figure 12: (a) Cumulative seismic moment for the events plotted in Fig. 11a, as a function of distance north from 35° N. Curve marked " M_0 " is for scalar moments and curve marked " M_{yy} " is for the component of the moment tensor that represents extension in a north-south direction. The difference between the two curves primarily represents the contribution from strike-slip events within the region.

(b-d) Comparison of the data of (a) with velocity profiles calculated along the y-axis of Fig. 3 for the calculations shown in Figs. 6 and 8. The seismic data from (a) are normalized so that the cumulative moment, whether M_0 or M_{yy} , is unity at the north of the region. Calculated velocity profiles are labelled with the Peclet number for the calculation and Q/RT_L is 50 in (b), 25 in (c), and 12.5 in (d).

Figure 13: Paleomagnetic rotations determined for locations in the Aegean. Wedges show the α_{95} range about the mean direction. I, Ionian islands (Kefalonia, Corfu, Zakynthos); E, Epirus-Akarnania; V, Volos; Ch, Chalkidiki peninsula; Ev, Evia; S, Skyros; T, Thrace; L, Lesbos; R, Rhodes; C, Crete; Iz, Izmir.

Figure 14: Calculated finite rotations at an elapsed time of 13 Ma for selected experiments. Vectors show the amount of rotation, with the zero rotation

direction being north (towards the top of the page). Rotations less than 5° are not plotted.

Table captions

Table 1: Summary of dimensionless parameters and the ranges of values used in the calculations.

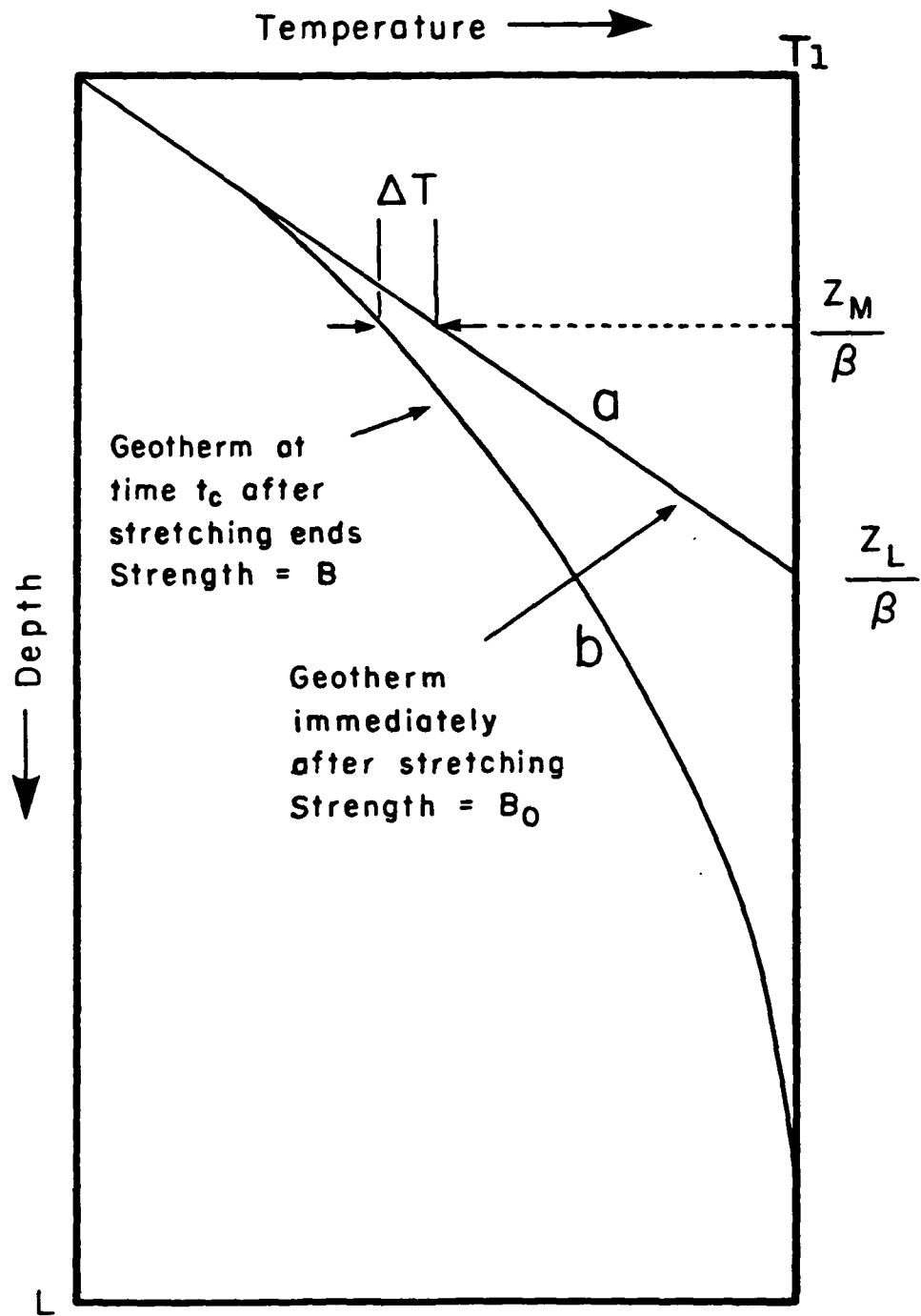
Table 2: Values of constants used in the calculations.

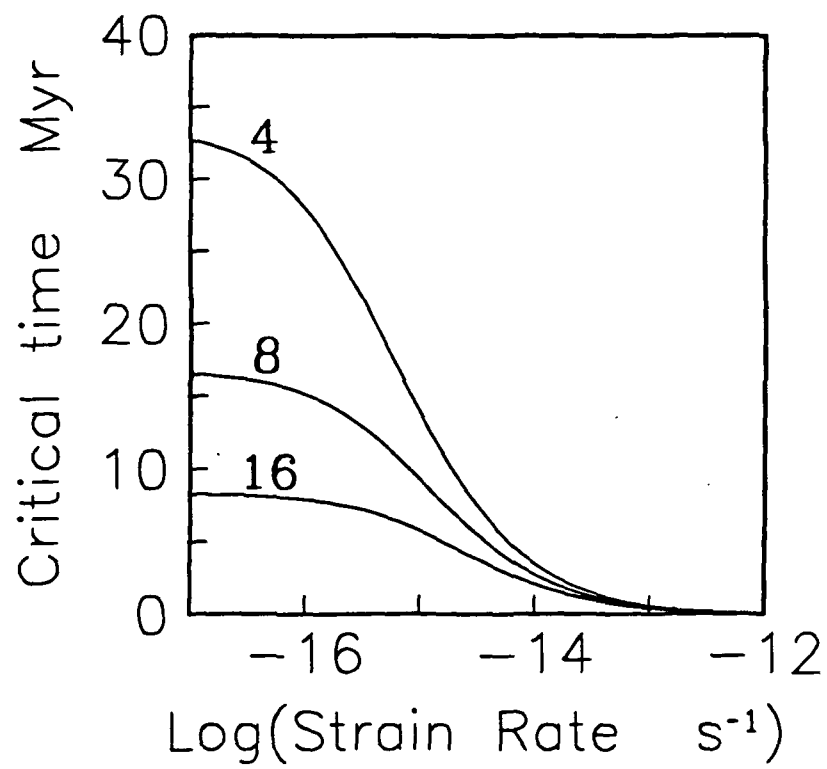
Table 1

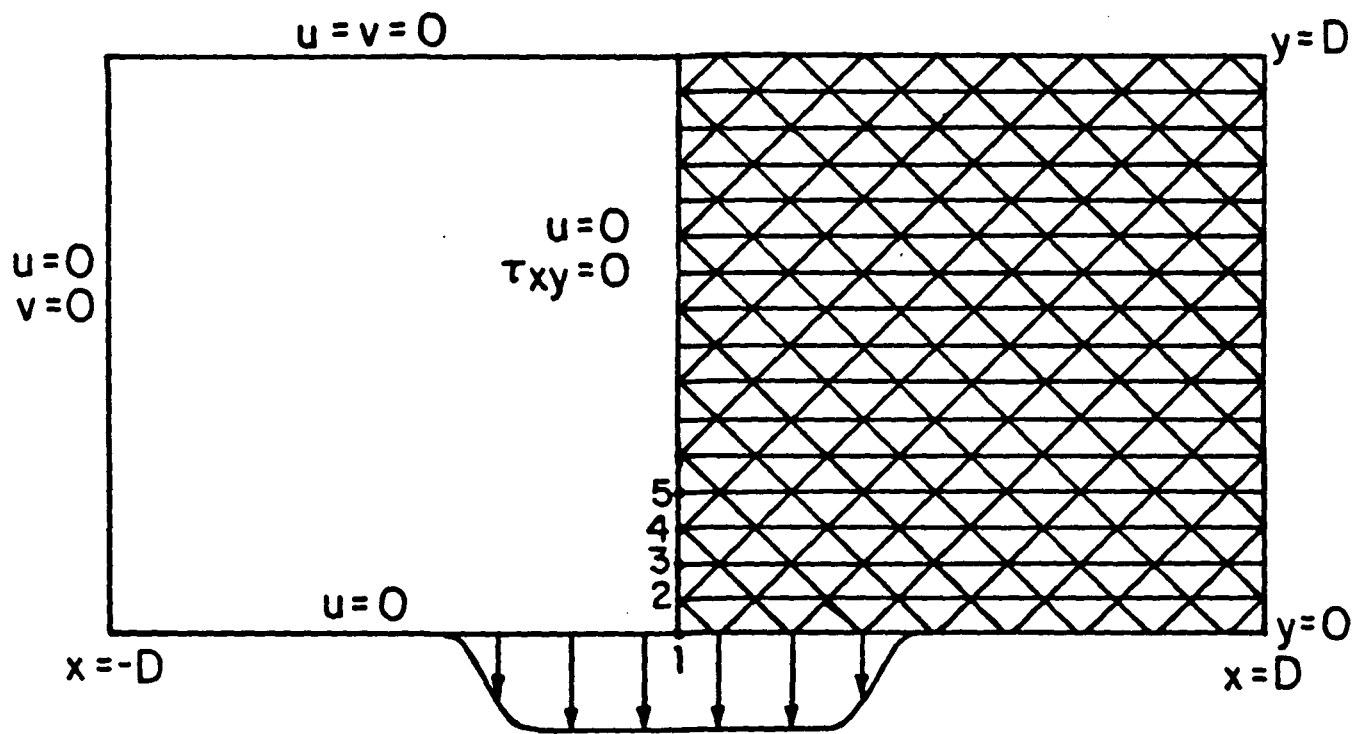
Parameter	Description	Value
Pe	Peclet number	300, 1000, 3000
Q/RT_L	temperature dependence	12.5, 25, 50
Ar	Argand number	-3, 0, 3
n	stress exponent	3

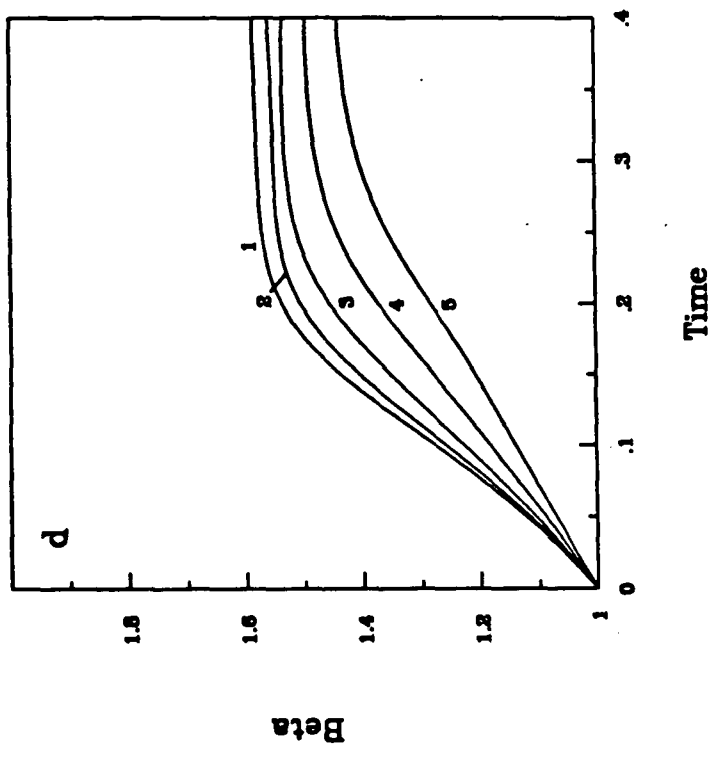
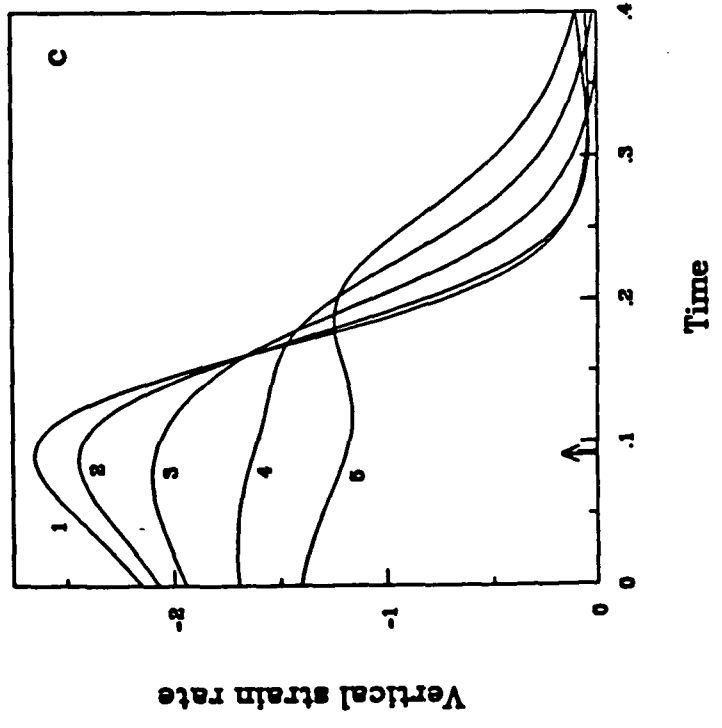
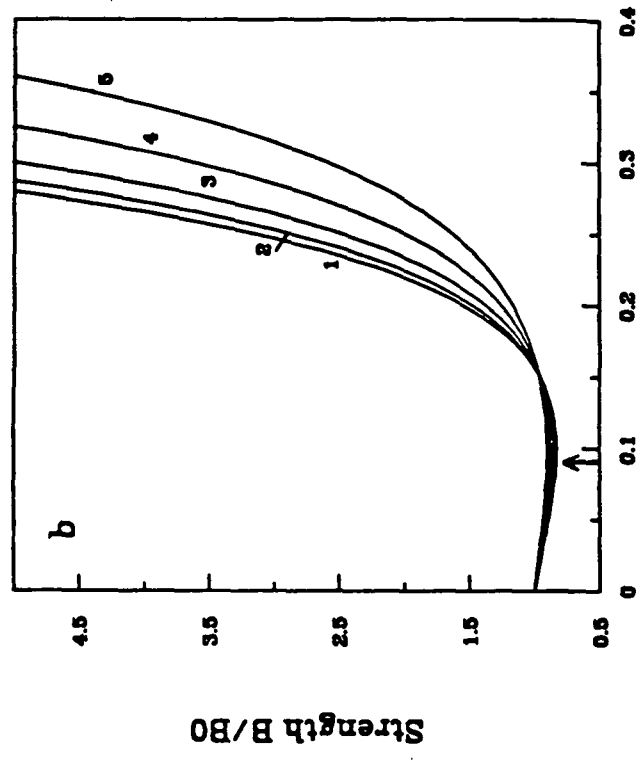
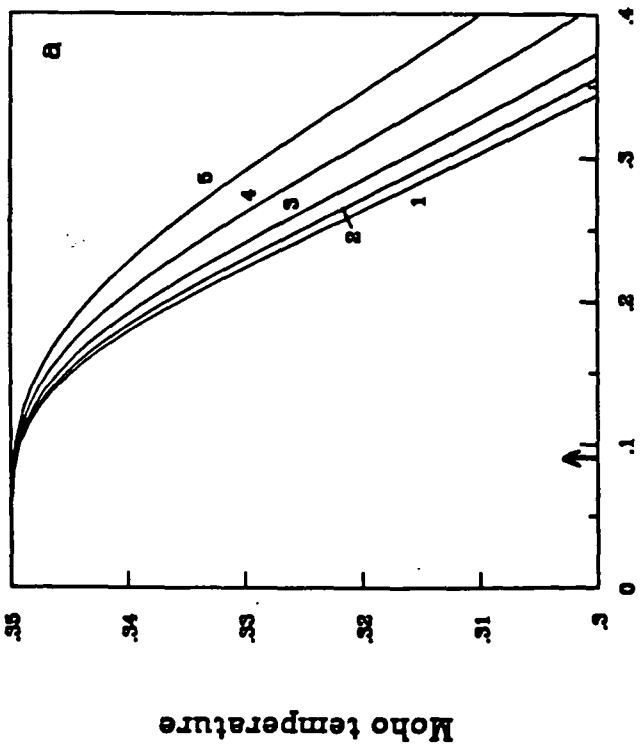
Table 2

Parameter	Description	Value
D	horizontal scale length	1000 km
L_0	lithosphere thickness	100 km
S_0	initial crustal thickness	35 km
t_0	time constant ($= D / v_0$)	33 Ma
ρ_c	density of crust	$3.0 \times 10^3 \text{ kg m}^{-3}$
ρ_m	density of mantle	$3.3 \times 10^3 \text{ kg m}^{-3}$
g	gravitational acceleration	9.8 m s^{-2}
T_L	reference temperature	1400 C
κ	thermal diffusivity	$10^{-6} \text{ m}^2 \text{ s}^{-1}$
R	gas constant	$8.31 \times 10^{-3} \text{ kJ mol}^{-1} \text{ K}^{-1}$



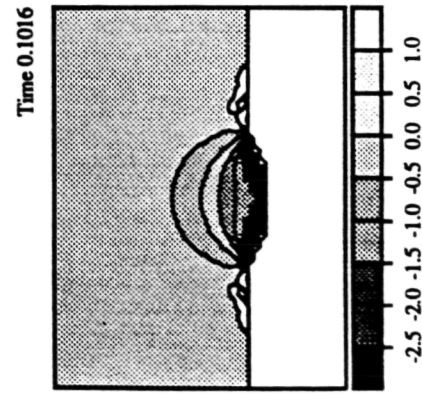
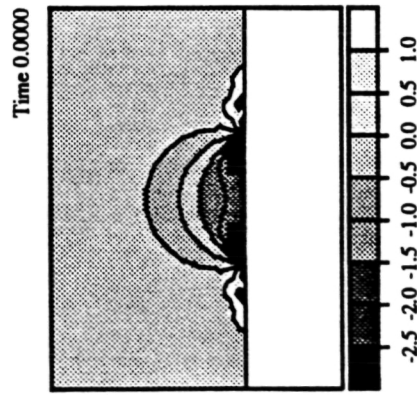
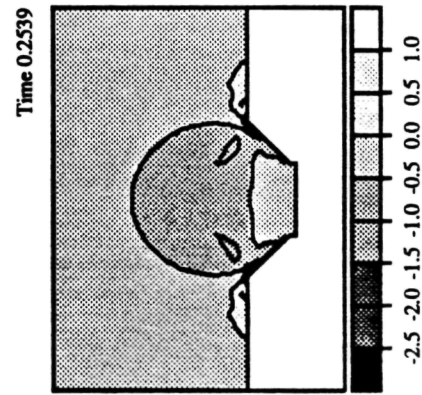
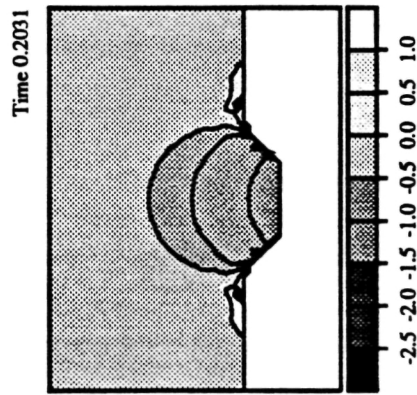
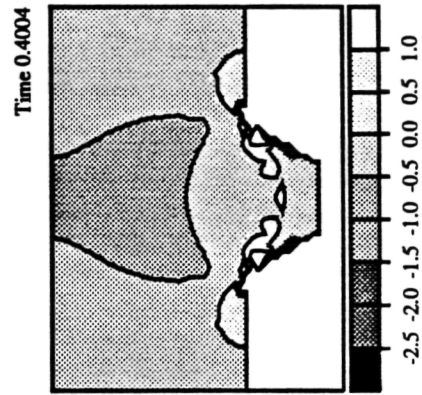
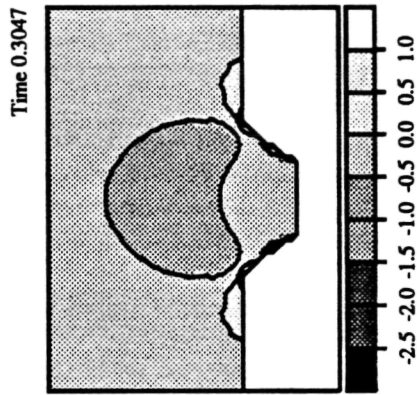






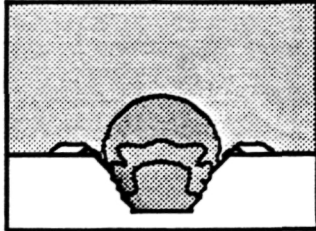
Peclet Number = 300; $Q/RT = 50$; $n = 3$; $Ar = 0$

ORIGINAL PAGE IS
OF POOR QUALITY



Strain Rates at Dimensionless Time 0.4

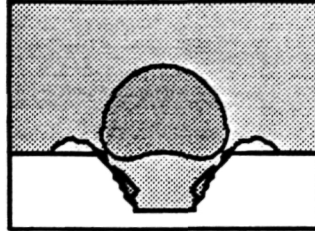
Pe = 300; Q/RT = 12.5



-2.5 -2.0 -1.5 -1.0 -0.5 0.0 0.5 1.0

Vertical Strain Rate

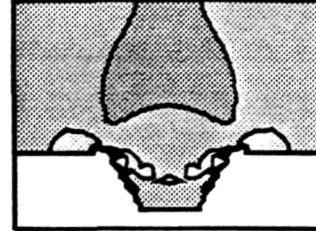
Pe = 300; Q/RT = 25



-2.5 -2.0 -1.5 -1.0 -0.5 0.0 0.5 1.0

Vertical Strain Rate

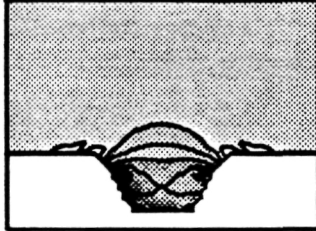
Pe = 300; Q/RT = 50



-2.5 -2.0 -1.5 -1.0 -0.5 0.0 0.5 1.0

Vertical Strain Rate

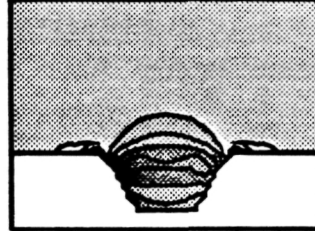
Pe = 1000; Q/RT = 12.5



-2.5 -2.0 -1.5 -1.0 -0.5 0.0 0.5 1.0

Vertical Strain Rate

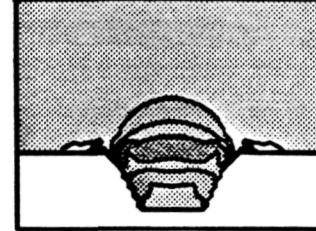
Pe = 1000; Q/RT = 25



-2.5 -2.0 -1.5 -1.0 -0.5 0.0 0.5 1.0

Vertical Strain Rate

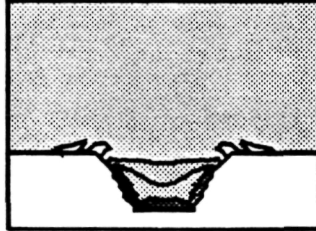
Pe = 1000; Q/RT = 50



-2.5 -2.0 -1.5 -1.0 -0.5 0.0 0.5 1.0

Vertical Strain Rate

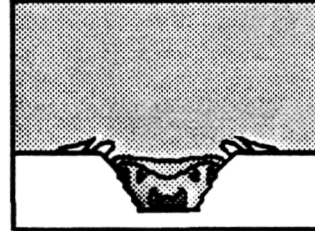
Pe = 3000; Q/RT = 12.5



-5.0 -4.0 -3.0 -2.0 -1.0 0.0 1.0 2.0

Vertical Strain Rate

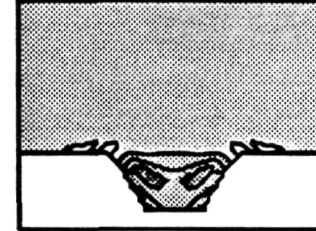
Pe = 3000; Q/RT = 25



-5.0 -4.0 -3.0 -2.0 -1.0 0.0 1.0 2.0

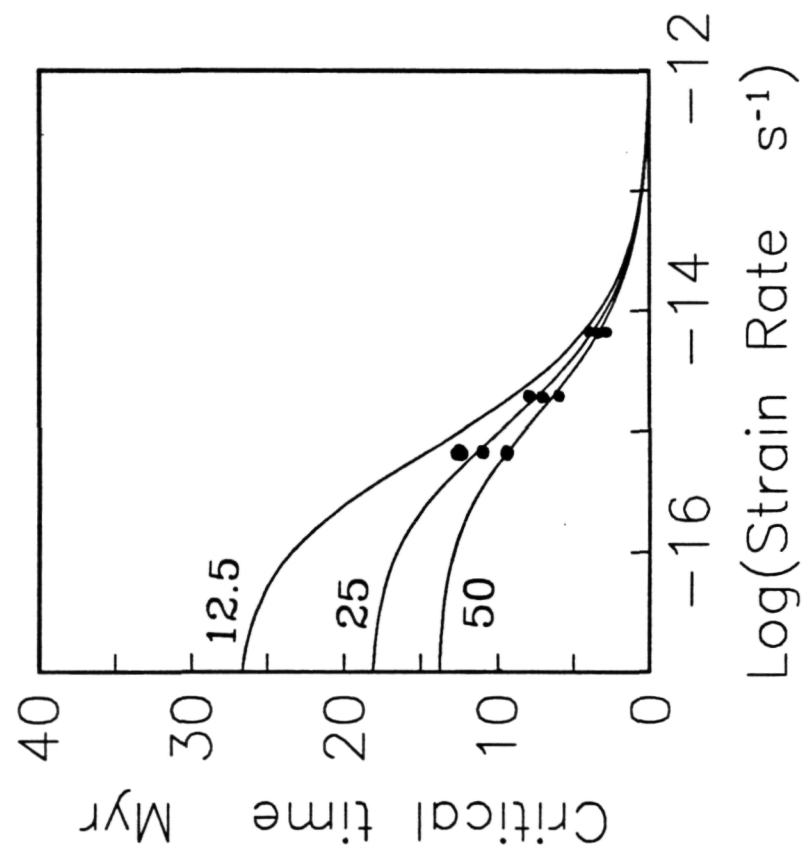
Vertical Strain Rate

Pe = 3000; Q/RT = 50



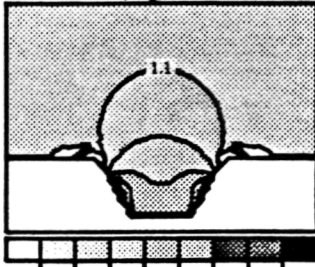
-5.0 -4.0 -3.0 -2.0 -1.0 0.0 1.0 2.0

Vertical Strain Rate



Extensional Strains at Dimensionless Time 0.4

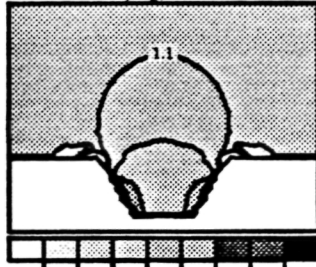
Pe = 300; Q/RT = 12.5



0.5 1.0 1.5 2.0 2.5 3.0 3.5 4.0

Beta

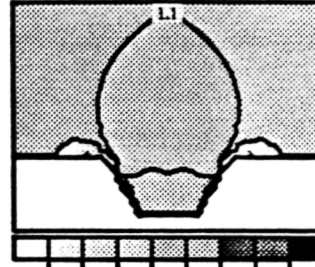
Pe = 300; Q/RT = 25



0.5 1.0 1.5 2.0 2.5 3.0 3.5 4.0

Beta

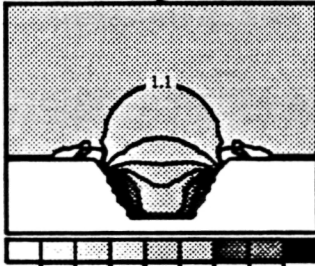
Pe = 300; Q/RT = 50



0.5 1.0 1.5 2.0 2.5 3.0 3.5 4.0

Beta

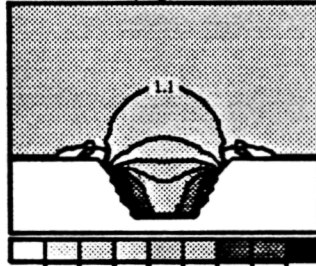
Pe = 1000; Q/RT = 12.5



0.5 1.0 1.5 2.0 2.5 3.0 3.5 4.0

Beta

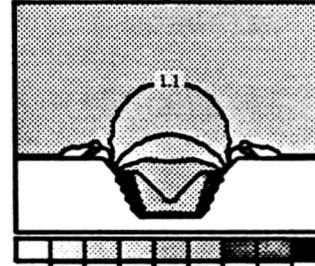
Pe = 1000; Q/RT = 25



0.5 1.0 1.5 2.0 2.5 3.0 3.5 4.0

Beta

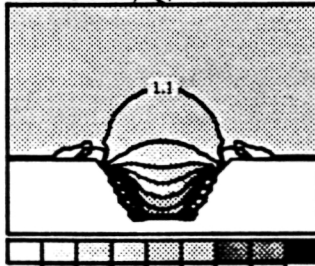
Pe = 1000; Q/RT = 50



0.5 1.0 1.5 2.0 2.5 3.0 3.5 4.0

Beta

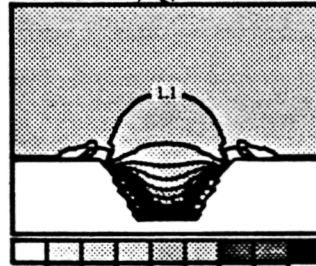
Pe = 3000; Q/RT = 12.5



0.5 1.0 1.5 2.0 2.5 3.0 3.5 4.0

Beta

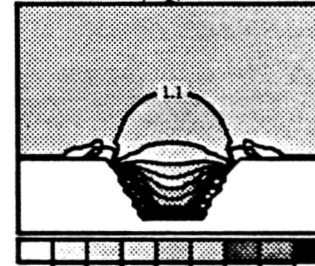
Pe = 3000; Q/RT = 25



0.5 1.0 1.5 2.0 2.5 3.0 3.5 4.0

Beta

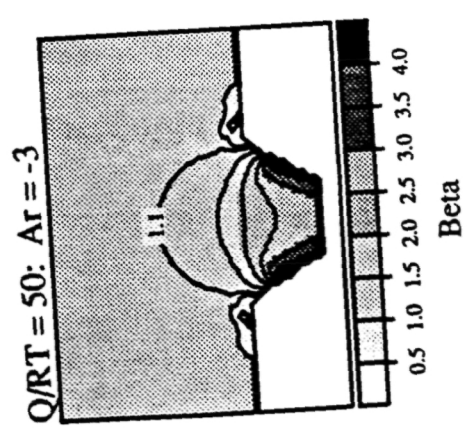
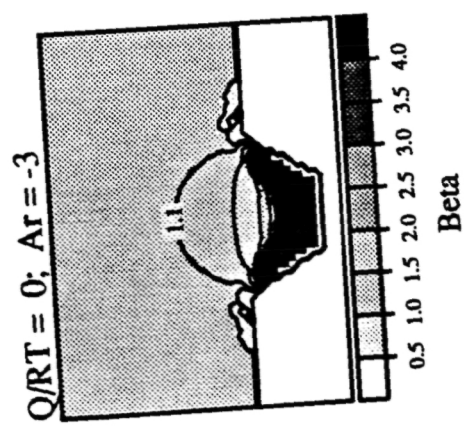
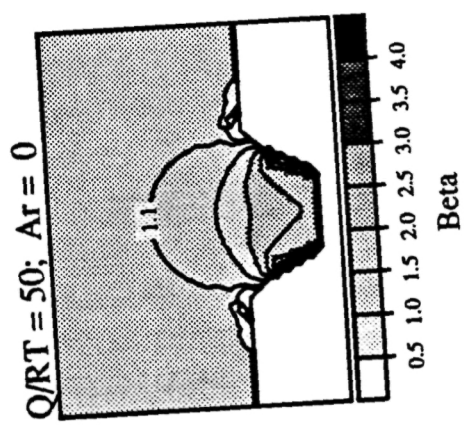
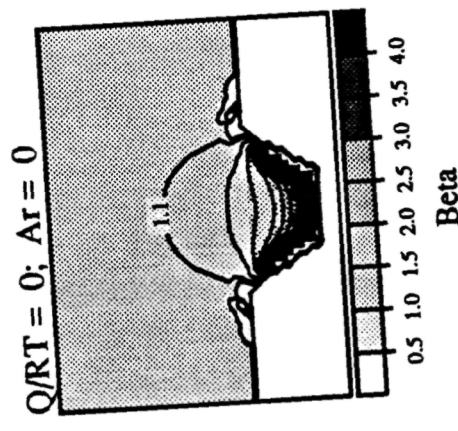
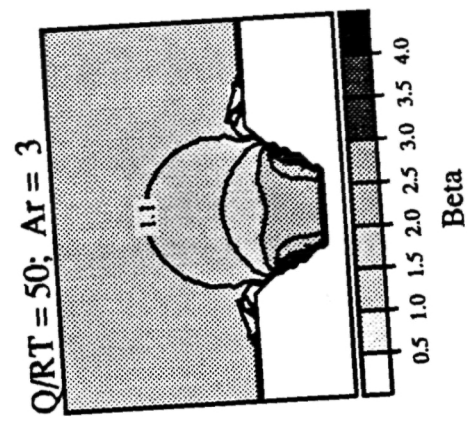
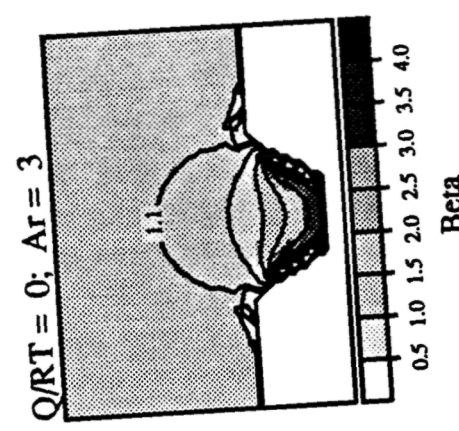
Pe = 3000; Q/RT = 50



0.5 1.0 1.5 2.0 2.5 3.0 3.5 4.0

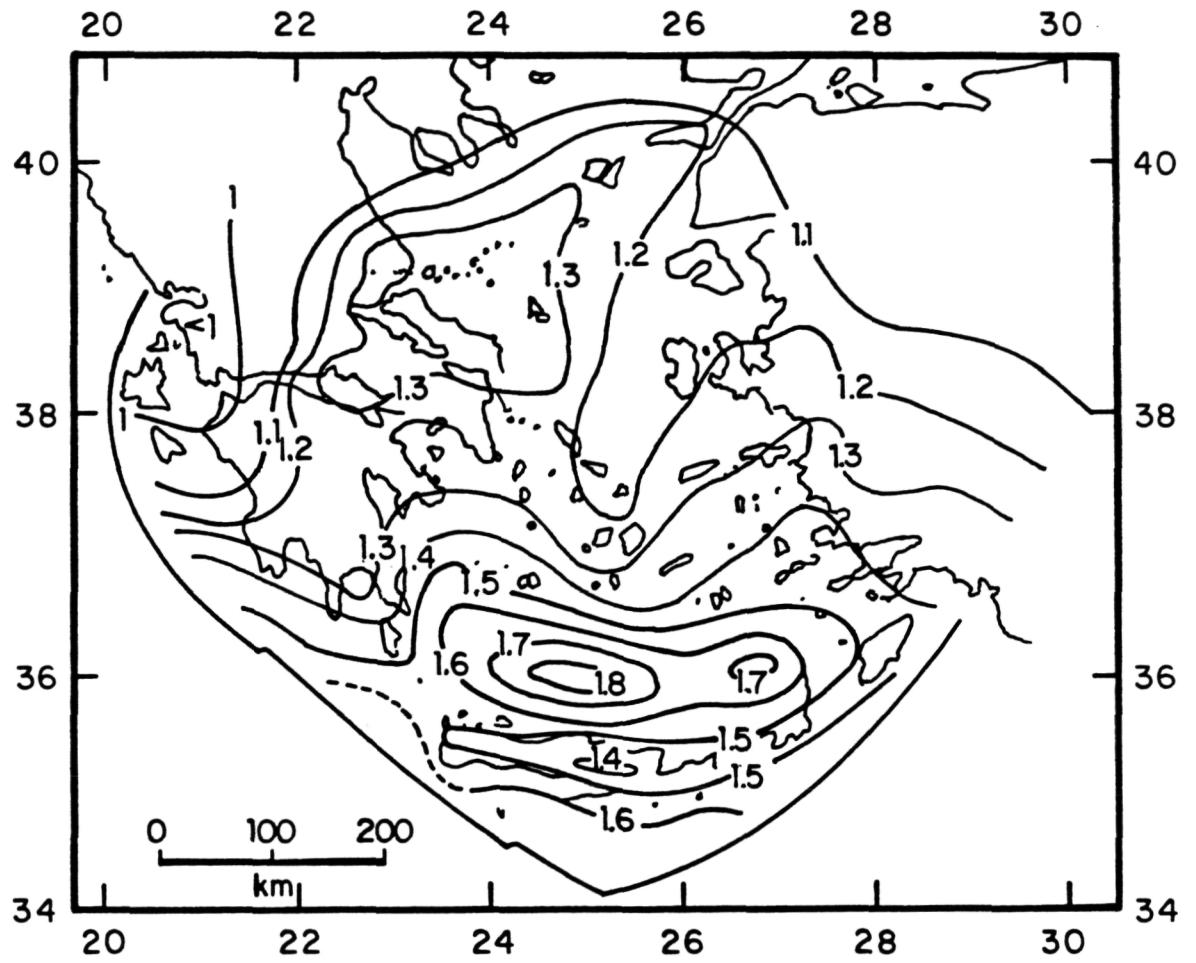
Beta

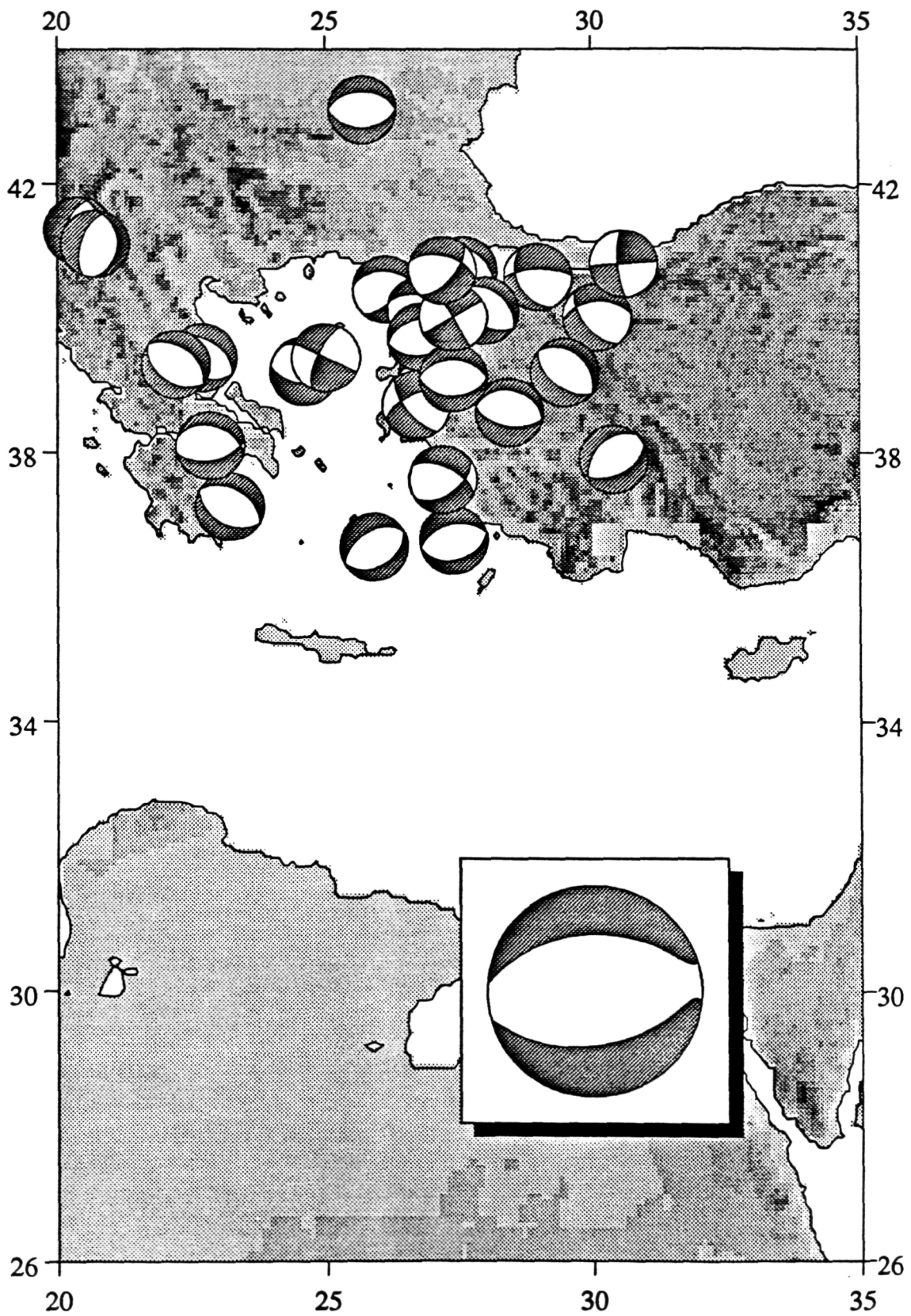
Extensional Strains at Dimensionless Time 0.4



a

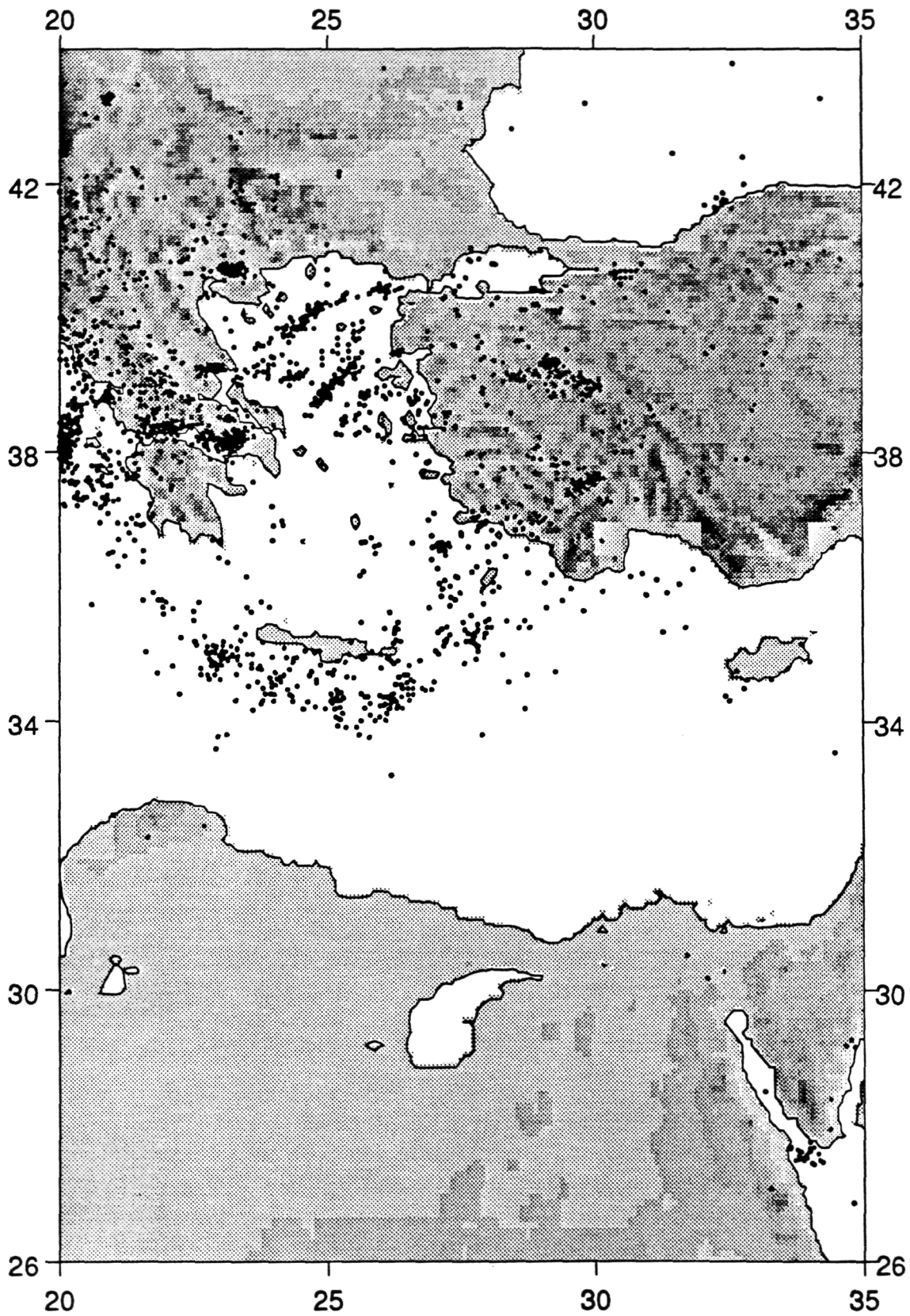
b

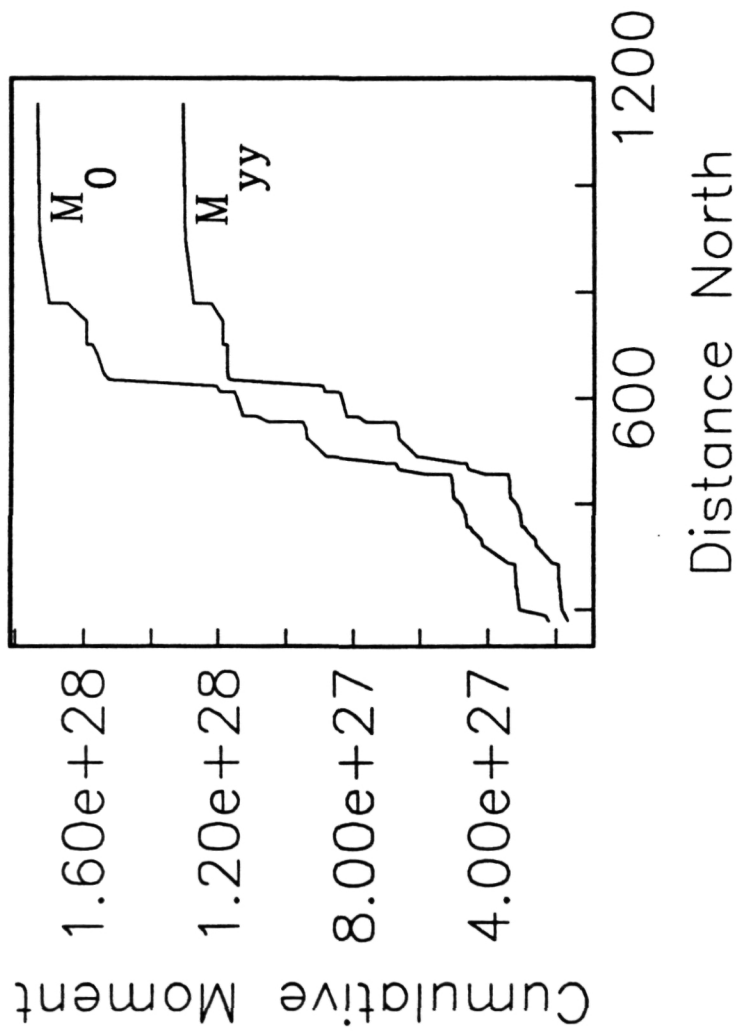




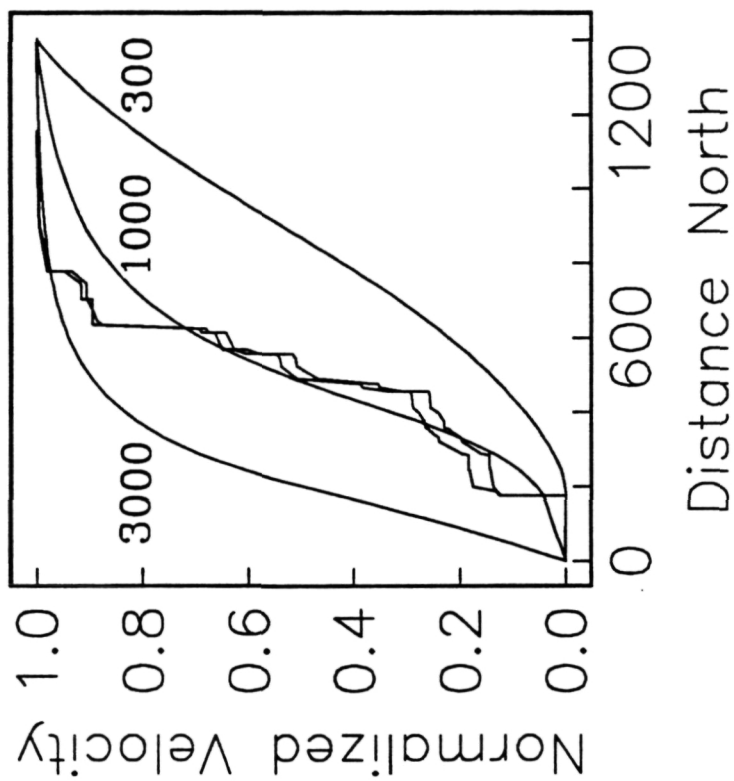
Aegean 1909 - 1981

ORIGINAL PAGE IS
OF POOR QUALITY

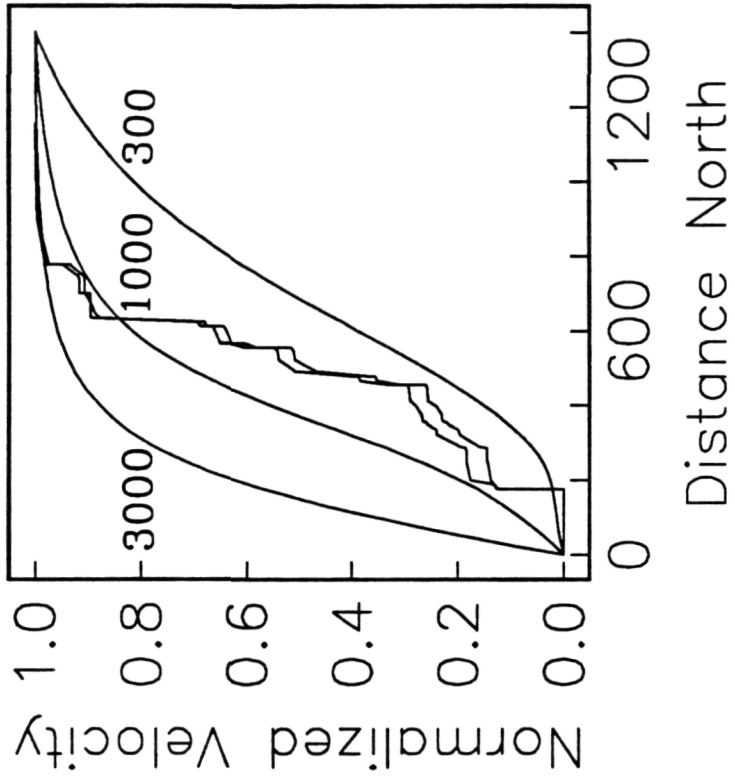




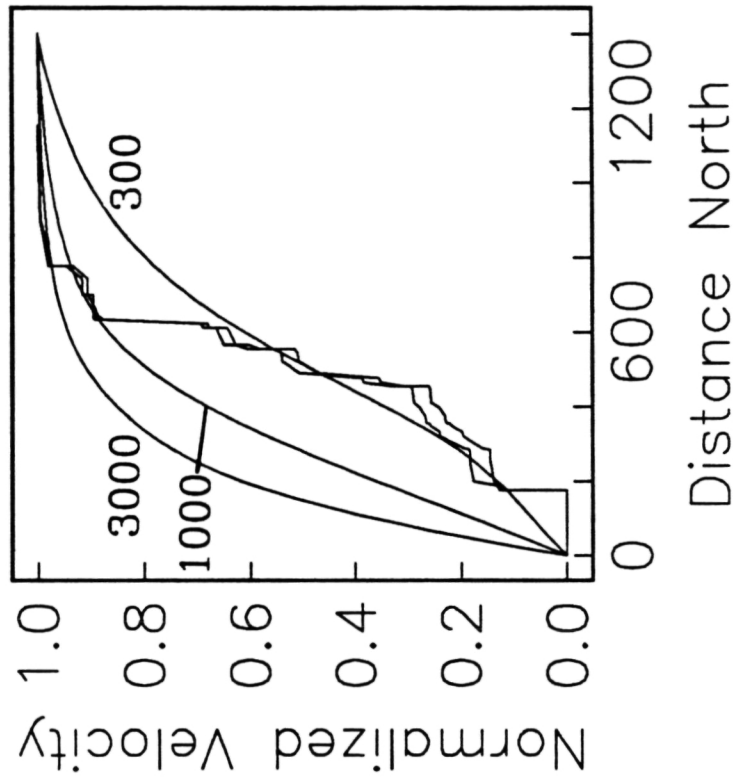
$n=3$ $Ar=3$ $Q/RT = 50$

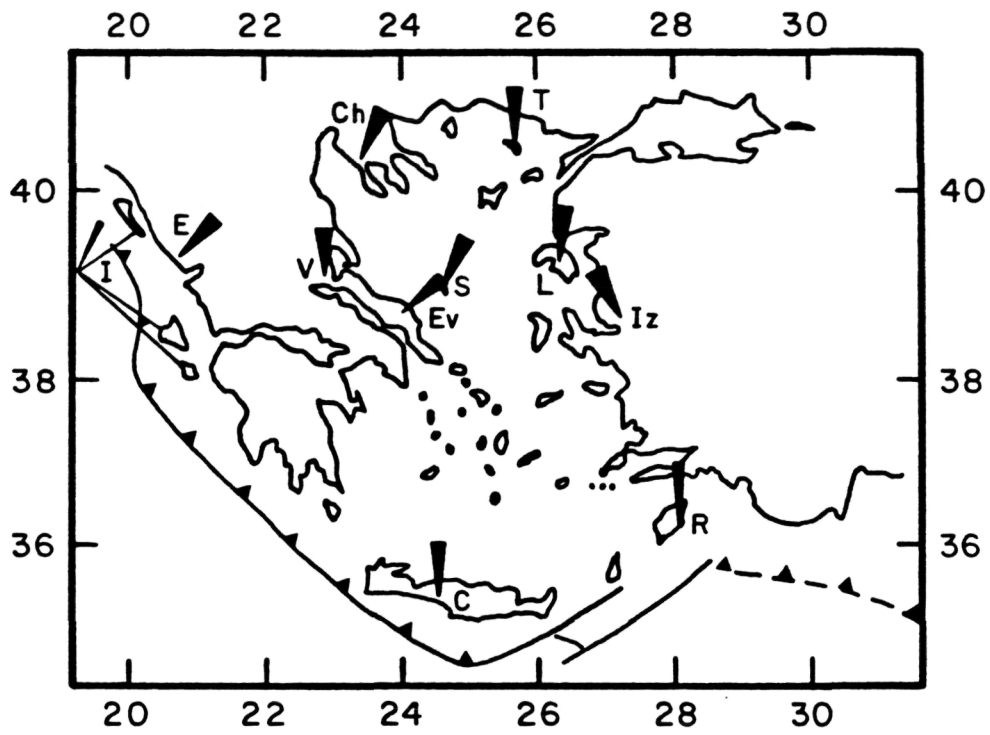


$n=3$ $Ar=3$ $Q/RT = 25$

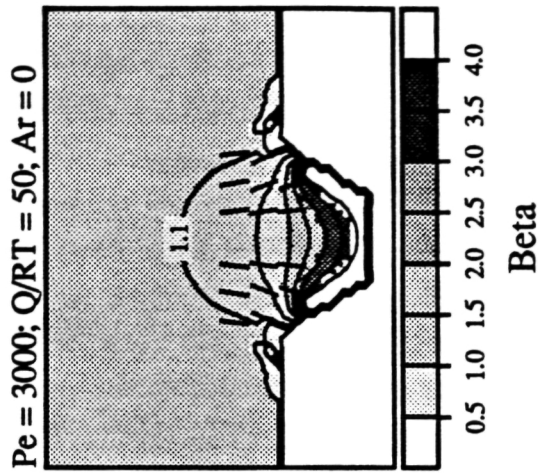
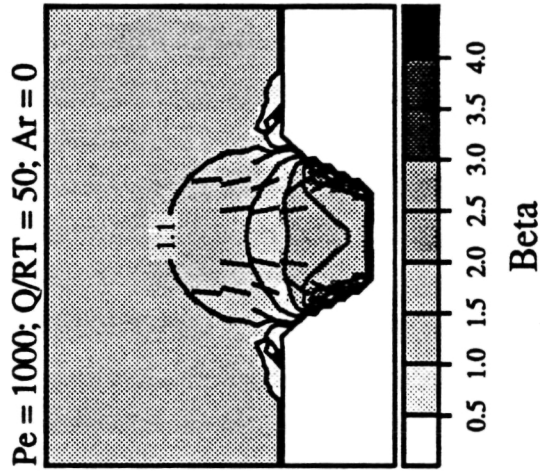
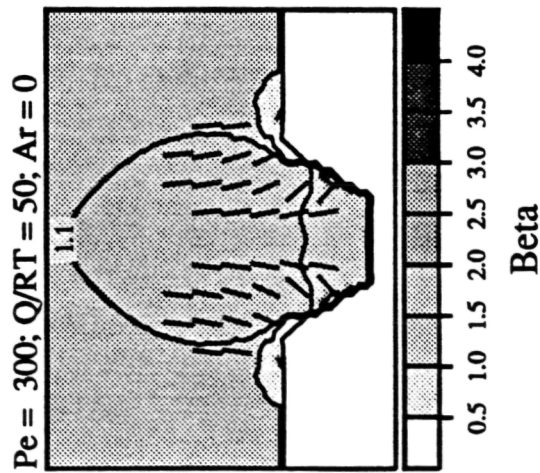


$n=3$ $Ar=3$ $Q/RT = 12.5$





Rotations and Extensional Strain at Dimensionless Time 0.4



REFERENCES

- Angelier, J., N. Lyb ris, X. LePichon, E. Barrier, and P. Huchon, The tectonic development of the Hellenic arc and the Sea of Crete: 9 synthesis, *Tectonophysics*, 86, 159-196, 1982.
- Artyushkov, E. V., Stresses in the lithosphere caused by crustal thickness inhomogeneities, *J. Geophys. Res.*, 78, 7675-7708, 1973.
- Bird, P. and K. Piper, Plane-stress finite element models of tectonic flow in southern California, *Phys. Earth. Planet. Inter.*, 21, 158-175, 1980.
- Brace, W. F. and D. L. Kohlstedt, Limits on lithospheric stress imposed by laboratory experiments, *J. Geophys. Res.*, 85, 6248-6252, 1980.
- England, P. C., Constraints on extension of continental lithosphere, *J. Geophys. Res.*, 88, 1145-1152, 1983.
- England, P. C. and D. P. McKenzie, A thin viscous sheet model for continental deformation, *Geophys. J. R. astr. Soc.*, 70, 295-321, 1982.
- England, P. C. and D. P. McKenzie, Correction to: A thin viscous sheet model for continental deformation, *Geophys. J. R. astr. Soc.*, 73, 523-532, 1983.
- England, P. C., G. A. Houseman, and L. J. Sonder, Length scales for continental deformation in convergent, divergent, and strike-slip environments: Analytical and approximate solutions for a thin viscous sheet model, *J. Geophys. Res.*, 90, 3551-3557, 1985.
- Fleitout, L. and C. Froidevaux, Tectonics and topography for a lithosphere containing density heterogeneities, *Tectonics*, 1, 21-57, 1982.
- Fletcher, R. C. and B. Hallet, Unstable extension of the lithosphere: A mechanical model for basin-and-range structure, *J. Geophys. Res.*, 88, 7457-7466, 1983.
- Goetze, C., The mechanisms of creep in olivine, in: **Creep of Engineering Materials and the Earth**, *Phil. Trans. Roy. Soc. London Ser. A.*, 288, 99-119, 1978.
- Homer, F. and R. Freeman, Palaeomagnetic evidence from pelagic limestones for clockwise rotation of the Ionian zone, western Greece, *Tectonophysics*, 98, 11-27, 1983.
- Horvath, F. and H. Berckhemer, Mediterranean backarc basins, in: **Alpine-Mediterranean Geodynamics**, H. Berckhemer and K. Hsu, eds., *AGU Geodynamics Series*, 7, 141-173, 1982.
- Houseman, G. A. and P. C. England, A dynamical model of lithosphere extension and sedimentary basin formation, *J. Geophys. Res.*, 91, 719-729, 1986a.
- Houseman, G. A. and P. C. England, Finite strain calculations of continental deformation: 1. Method and general results for convergent zones, *J. Geophys. Res.*, 91, 3651-3663, 1986b.
- Jackson, J. A. and D. P. McKenzie, in preparation, 1988.
- Jarvis, G. T. and D. P. McKenzie, The development of sedimentary basins with finite extension times, *Earth Planet. Sci. Lett.*, 48, 42-52, 1980.

- Kissel, C., C. Laj, and A. Mazaud, First paleomagnetic results from Neogene formations in Evia, Skyros, and the Volos region and the deformation of central Aegea, *Geophys. Res. Lett.*, *13*, 1446-1449, 1986a.
- Kissel, C., C. Laj, and C. Müller, Tertiary geodynamical evolution of northwestern Greece: Paleomagnetic results, *Earth Planet. Sci. Lett.*, *72*, 190-204, 1985.
- Kissel, C., C. Laj, A. Poisson, Y. Savascin, K. Simeakis, and J. L. Mercier, Paleomagnetic evidence for Neogene rotational deformations in the Aegean domain, *Tectonics*, *5*, 783-795, 1986b.
- Kondopoulou, D. and M. Westphal, Paleomagnetism of the tertiary intrusives from Chalkidiki (northern Greece), *J. Geophys.*, *59*, 62-66, 1986.
- Laj, C., M. Jamet, D. Sorel, and J. P. Valenle, First paleomagnetic results from Mio-Pliocene series of the Hellenic sedimentary arc, *Tectonophysics*, *86*, 45-67, 1982.
- Le Pichon, X., Land-locked oceanic basins and continental collision, in: **Mountain Building Processes**, K. Hsü, ed., Academic Press, London, 1983.
- LePichon, X. and J. Angelier, The Hellenic arc and trench system: A key to the neotectonic evolution of the eastern Mediterranean area, *Tectonophysics*, *60*, 1-42, 1979.
- Le Pichon, X. and J.-C. Sibuet, Passive margins: A model of formation, *J. Geophys. Res.*, *86*, 3708-3720, 1981.
- Makris, J., Crustal structure of the Aegean Sea and the Hellenides obtained from geophysical surveys, *J. Geophys.*, *41*, 441-443, 1975.
- Makris, J. and R. Veis, Crustal structure of the central Aegean Sea and the islands of Evia and Crete, Greece, obtained by refractonal seismic experiments, *J. Geophys. Res.*, *42*, 329-341, 1977.
- McKenzie, D. P., Some remarks on the development of sedimentary basins, *Earth Planet. Sci. Lett.*, *40*, 25-32, 1978a.
- McKenzie, D. P., Active tectonics of the Alpine-Himalayan belt: The Aegean Sea and surrounding regions, *Geophys. J., R. astr. Soc.*, *55*, 217-254, 1978b.
- McKenzie, D. P., and J. A. Jackson, The relationship between strain rates, crustal thickening, palaeomagnetism, finite strain, and fault movements within a deforming zone, *Earth Planet. Sci. Lett.*, *65*, 182-202, 1983.
- Royden, L. and C. E. Keen, Rifting process and thermal evolution of the continental margin of eastern Canada determined from subsidence curves, *Earth Planet. Sci. Lett.*, *51*, 343-361, 1980.
- Royden, L., F. Horvath, A. Nagymarasy, and L. Stegena, Evolution of the Pannonian basin system: Subsidence and thermal history, *Tectonics*, *2*, 91-137, 1983.
- Sclater, J. G. and P. A. F. Christie, Continental stretching: An explanation of the post-mid-Cretaceous subsidence of the central North Sea basin, *J. Geophys. Res.*, *85*, 3711-3739, 1980.

- Sonder, L. J. and P. C. England, Vertical averages of rheology of the continental lithosphere: Relation to thin sheet parameters, *Earth Planet. Sci. Lett.*, 77, 81-90, 1986.
- Sonder, L. J., P. C. England, B. P. Wernicke, and R. L. Christiansen, A physical model for Cenozoic extension of western North America, in: **Continental Extensional Tectonics**, J. F. Dewey and P. L. Hancock, Eds., *Geol. Soc. London Special Pub.*, 28, 187-201, 1987.
- Valente, J. P., C. Laj, D. Sorel, S. Roy, and J.-P. Valet, Paleomagnetic results from Mio-Pliocene marine sedimentary series in Crete, *Earth Planet. Sci. Lett.*, 57, 159-172, 1982.
- Vilotte, J. P., M. Daignières, and R. Madariaga, Numerical modeling of intraplate deformation: Simple mechanical models of continental collision, *J. Geophys. Res.*, 87, 10709-10728, 1982.
- Vilotte, J. P., R. Madariaga, M. Daignières, and O. Zienkiewicz, Numerical study of continental collision: Influence of buoyancy forces and an initial stiff inclusion, *Geophys. J. R. astr. Soc.*, 84, 279-310, 1986.
- Zuber, M. T. and E. M. Parmentier, Lithospheric necking: A dynamic model for rift morphology, *Earth Planet. Sci. Lett.*, 77, 373-383, 1986.
- Zuber, M. T., E. M. Parmentier, and R. C. Fletcher, Extension of continental lithosphere: A model for two scales of basin and range deformation, *J. Geophys. Res.*, 91, 4826-4838, 1986.